The Uses of Isothermal Plastometry

William G. Lloyd,* John W. Reasoner,* James C. Hower** and Linda P. Yates**

*Department of Chemistry, Western Kentucky University, Bowling Green, KY 42101

**Institute for Mining and Minerals Research, University of Kentucky, Lexington, KY 40506

The most widely used characterization of coal fluidity is the plastometric method developed by Gieseler (1). In a modified form, with a torque clutch replacing the original pulleys and weights, this has become a standard American procedure (2). Its relationship to dilatometry is well established (3-6).

The standard 3 deg/min Gieseler analysis provides a fixed-angle 'slice' across the fluidity-temperature surface, and in a single determination may provide plasticity information across a span of 50-100 deg C. It often reveals fluidity differences of more than a thousandfold among coals of similar rank and chemical composition.

There are, however, several advantages to be gained by conducting Gieseler analyses under isothermal conditions. The resulting data permit the estimation of 'melting' and 'coking' rates and hence (from several runs at different temperatures) the determination of temperature dependencies of these rates. Isothermal data generally provide better simulation of the fluidity characteristics of coal in an actual continuous process such as extrusion feeding (7-9). Isothermal data clearly distinguish among coals of differing temperatures of maximum fluidity.

Fitzgerald has shown that when ln(fluidity) is plotted against time under isothermal conditions the coking slope is substantially linear. The coking slopes of a group of English coals in his study exhibit Arrhenius temperature dependencies, with activation energies in the vicinity of 50 kcal (10,11).

We have confirmed these observations for a group of 29 hvb coals from the eastern mid-continent beds. For most of these coals the isothermal melting curve is also found to be substantially linear (12,13). Figure 1 illustrates a typical isothermal run. The data provide not only classical information (softening point, time of maximum fluidity, solidification point and maximum observed fluidity) but also estimates of the melting and coking slopes and an additional measure, intersection maximum fluidity. This last is obtained by extrapolation of the two slopes to their point of intersection.

Intersection maximum fluidity has several advantages over observed maximum fluidity. Some coals have a flattish and poorly defined region of maximum fluidity. Coals which outgas vigorously are likely to produce irregular and irreproducible readings in the vicinity of maximum fluidity. Highly plastic coals may develop fluidity in excess of 30,000 ddpm, greater than can be measured by the Gieseler plastometer. In all such cases the intersection maximum fluidity is accessible and in our experience is a more consistent and reproducible measure, even for the case of ASTM temperature-gradient runs (Figure 2).

In the present study a number of freshly sampled coals from active mines and coal cleaning plants have been obtained and reduced, stored under inert gas at -40°, and then analyzed using a research model Gieseler plastometer (Standard Instrumentation), sensitive to 0.1 ddpm (roughly 100 megapoise for a Newtonian fluid). Three of these coals are characterized in Table 1.

When a coal is examined in a series of isothermal runs, both melting and coking slopes are steeper at higher temperatures. These trends are illustrated in Figure 3. For this moderately plastic coal, maximum fluidity is increased over tenfold by raising temperature from 412 to 431°C.

Figure 4 is an Arrhenius plot based upon 20 isothermal runs at 412-438°C with Coal #41. The top slope shows the variation of ln ln(intersection maximum fluidity) with reciprocal temperature. The middle and lower slopes show the corresponding variations of ln(melting slope) and ln(coking slope). Each of these is essentially linear over the experimental range.

During an isothermal Gieseler run the solder-pot furnace maintains a nearly constant temperature (standard deviation less than 1.0°C). The linearity of the Arrhenius slopes permits the determination of activation energies with fairly good precision (Table 2). The Arrhenius relationship also permits the interpolation of data so that slopes and fluidities of a number of coals can be determined at precisely the same temperature.

Overall isothermal fluidity characteristics of these and other coals which we are studying (14) are summarized in Table 3. These data suggest some general trends among hvb coals. Activation energies of the coking slopes are all in the vicinity of 50 kcal, as Fitzgerald found with English coals (11). Coking slope values are slightly higher for the sparingly plastic coals. Activation energies of the melting slopes tend to increase with increasing plasticity, from 25-30 kcal for sparingly plastic coals to 50-55 kcal for highly plastic coals. Activation energies of ln(maximum fluidity) decrease with increasing plasticity, from 30-35 kcal for sparingly plastic coals to 10-20 kcal for highly plastic coals. The ratio (melting slope) / (coking slope) is notably higher for the highly plastic coals.

Maximum fluidities measured under isothermal conditions, at or near the ASTM temperature of maximum fluidity, are substantially greater than the corresponding ASTM maximum fluidities. For sparingly fluid coals the maximum isothermal fluidity is typically two- to three-fold that observed in an ASTM run. This ratio increases with coal fluidity, with values typically in the range 5-8 for moderately plastic (30-300 ddpm) coals. Table 4 summarizes this trend for 17 coals for which isothermal data have been obtained at or very near the ASTM temperature of maximum fluidity. For highly fluid coals the isothermal data was obtained at temperatures appreciably below T(max flu). The maximum fluidity obtained in an ASTM run can be matched in an isothermal run conducted at 10-15 deg C below the ASTM temperature of maximum fluidity.

Discussion.

Since a very large number of parallel reactions is involved in both the melting and coking regions of an isothermal run, it is reasonable to ask why - for a semilogarithmic plot or any other plot - the change in fluidity with time has domains of substantial linearity. The condition necessary to find linearity under some conditions is that the major contributing reactions be of the same kinetic order:

$$-d[B]/dt = w_1 k_1 [B]^n + w_2 k_2 [B]^n + \ldots \qquad (1)$$

where the w_i's and k_i's denote weighting factors and empirical rate constants.

The right-hand terms are then easily collected into a single term. The observation that plots of ln(fluidity) vs. time yield melting and coking slopes which are essentially linear suggests that Equation 1 is in fact followed.

This does not mean, as some have suggested, that isothermal coking is a set of first-order processes. Since slurry fluidity is not a linear function of fluid fraction, the coking process is not kinetically first-order. Further work is needed before kinetic dependencies can be inferred from these curves.

Since melting and coking slopes and ln(maximum fludity) all follow Arrhenius dependencies, the fluidity span (the time interval during which fluidity exceeds a specified value) can also be calculated at any interpolated temperature. This can be seen analytically. If f is ln(intersection maximum fluidity), tm the time interval from initial softening to maximum fluidity and tc the time interval from maximum fluidity to coking point, then the melting slope m is equal to f/tm and the coking slope c is equal to f/tc. The total time span (tm + tc) is then:

$$t = f*(1/m + 1/c) \qquad (2)$$

If a process requires a minimum fluidity F' which is any value less than the maximum fludity, then:

$$t' = (f - f') * (1/m + 1/c) \qquad (3)$$

where $f' = \ln(F')$.

This study is part of an investigation into the predictability of plastic behavior in bituminous coals (14). We acknowledge with thanks the support of this work by the U.S. Department of Energy.

References

1. K. Gieseler, Gluckauf, 70, 178 (1934).
2. ASTM Method D2639, Amer. Soc. for Testing and Materials, Phila., PA, 1982.
3. D. W. van Krevelen, E. J. Huntjens and H. N. M. Dormans, Fuel, 35, 462 (1956).
4. R. Loison, A. Peytavy, A. F. Boyer and R. Grillot, in H. H. Lowry, ed., "Chemistry of Coal Utilization - Supplementary Volume", John Wiley & Sons, NY, 1963.
5. A. V. Khimichenko, et al., Khim. Tverd. Topl., 1971, 48.
6. W. R. K. Wu and W. H. Frederic, USBM Bulletin 661 (1971).
7. V. Kevorkian and F. J. Cumings, U.S. Patent 4,106,997 (1978).
8. P. R. Ryason and C. England, Fuel, 57, 241 (1978)
9. C. England, Proc. 17th Intersoc. Energy Conversion Conf., 2, 864 (1982).
10. D. Fitzgerald, Fuel, 35, 178 (1956).
11. D. Fitzgerald, Trans. Faraday Soc., 52, 362 (1956).
12. W. G. Lloyd, "Development of Methods of Characterizing Coal in its Plastic State", final rept., Caltech contract #954, 920 (1978).
13. W. G. Lloyd, H. E. Francis, M. R. Yewell, Jr., R. D. Kushida and V. D. Sankur, Amer. Chem. Soc. Divn. Fuel Chem. Preprints, 25 (2), 128 (1980).
14. W. G. Lloyd, J. W. Reasoner, J. C. Hower and L. P. Yates, "Predictors of Plasticity in Bituminous Coals", USDOE Contract DE-FG22-81PC40793.
15. Idem, ref. 14, Techn. Progr. Rept. 7, June 1983.

Table 1
Coal Characterization Data*

	Coal #18	Coal #22	Coal #41
County	Muhlenberg	Union	Butler
Seam and rank	KY #9, hvBb	KY #6, hvAb	Amos, hvBb
Moisture	7.09%	2.40%	7.78%
Ash	8.36	9.60	2.77
Volatile matter	40.6	39.4	42.1
% Carbon	74.1	76.0	80.7
% Hydrogen	5.11	5.42	5.74
% Nitrogen	1.50	1.44	1.61
% Sulfur	3.59	2.91	1.06
Heating value, Btu/lb	13,020	13,490	14,280
Free swelling index	4.5	8.	3.
% Vitrinite	76.1%	70.7%	79.0%
% Pseudovitrinite	1.2	5.3	6.7
% Exinite	3.5	3.2	6.3
% Resinite	0.4	0.5	0.9
% Fusinite	3.3	3.5	0.4
% Semifusinite	3.6	2.8	0.7
% Micrinite	1.7	1.9	2.7
% Macrinite	0.2	0.1	0.0
Mineral matter (Parr)	11.0	12.0	3.3
Vitrinite max reflect	0.54	0.73	0.67
ASTM Gieseler data:			
T(softening)**	388	376	398
T(max fluidity)	428	422-435	436
T(solidification)**	447	467	459
Max fluidity (observed)	26.8	>30,000	217
Max fluidity (intersctn)	44.5	2.61E+6	590

* Moisture is as determined, other values on a dry ash-included basis.
** Temperature at which fluidity value is 1.0 ddpm.

Table 2
Precision of Arrhenius Temperature Dependencies*

Coal	n	Melting slope	Coking slope	ln(Intersection max flu)
#18	20	31.0 ± 2.5	48.5 ± 3.2	35.9 ± 2.5
#22	19	56.5 ± 1.8	48.7 ± 2.0	20.0 ± 1.5
#41	20	43.8 ± 1.8	51.4 ± 2.0	19.7 ± 0.8

* Least-squares values in kcal and standard deviations.

Table 3

Fluidity Characteristics of Selected Coals*

Coals	Intersection max flu			Melting slope[1]			Coking slope[1]		
	400°C	420°C	E(a)	400°C	420°C	E(a)	400°C	420°C	E(a)
#22	2540	1.8E5	20.0	0.70	2.38	56.5	0.13	0.37	48.7
average of 5 other highly plastic coals	14300	2.5E5	12.3	0.99	3.0	51.	0.16	0.43	44.5
#41	40	277	19.7	0.24	0.62	43.8	0.14	0.43	51.4
average of 5 other medium plastic coals	40	366	21.4	0.34	0.82	42.1	0.19	0.53	48.7
#18	8	88	35.9	0.40	0.77	31.0	0.27	0.77	48.5
average of 5 other slightly plastic coals	5	24	33.2	0.35	0.62	26.9	0.20	0.60	50.8

* Fluidity averages are logarithmic. Properties averaged from coals 21, 25, 27, 32 and 34 (highly plastic); 15, 26, 36, 37 and 39 (medium plastic); and 02, 03, 09, 24 and 40 (slightly plastic), ref. 15.

[1] Slopes are in reciprocal minutes.

Table 4

Maximum Observed Fluidities under ASTM and Isothermal Conditions

no. of coals	Maximum fluidity (MF) range, ddpm	ASTM Conditions		Isothermal Conditions		Ratio*
		Avg MF	Avg T	Avg MF	Avg T	
5	2 < MF < 8	3.8	422°	10.2	421°	2.7
6	8 < MF < 32	12.8	426°	51.2	426°	4.0
6	32 < MF < 256	136.	430°	829.	430°	6.1

* Ratio of (maximum isothermal fluidity) / (maximum ASTM fluidity)

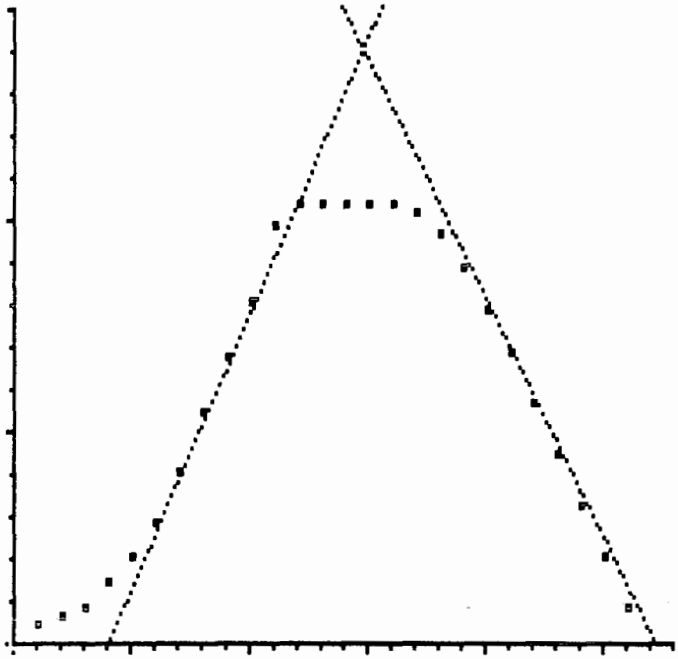

FIGURE 2. ASTM PLASTOMETRY OF A hvAb COAL. Horizontal: time in minutes, scale 0 to 28. Vertical: ln(fluidity in ddpm), scale 0 to 15. The flat top of the experimental curve marks the instrument limit of 30,000 ddpm.

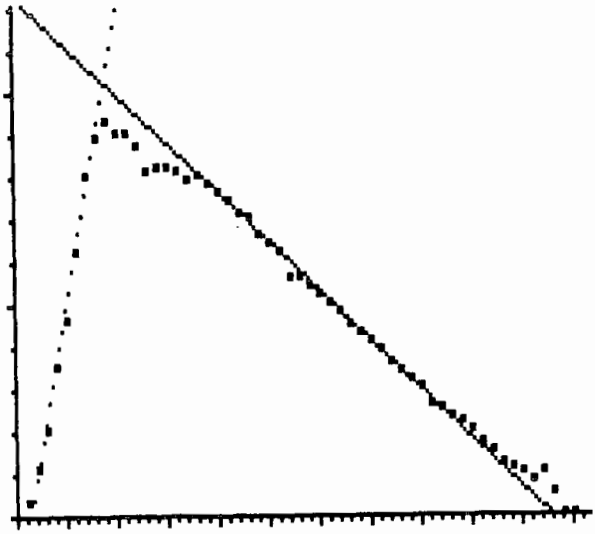

FIGURE 1. ISOTHERMAL PLASTOMETRY OF A hvAb COAL AT 405°C. Horizontal: time in minutes, scale 0 to 56. Vertical: ln(fluidity in ddpm), scale 0 to 12. Slope calculations use fluidities above 10 ddpm and below one quarter of the observed maximum fluidity.

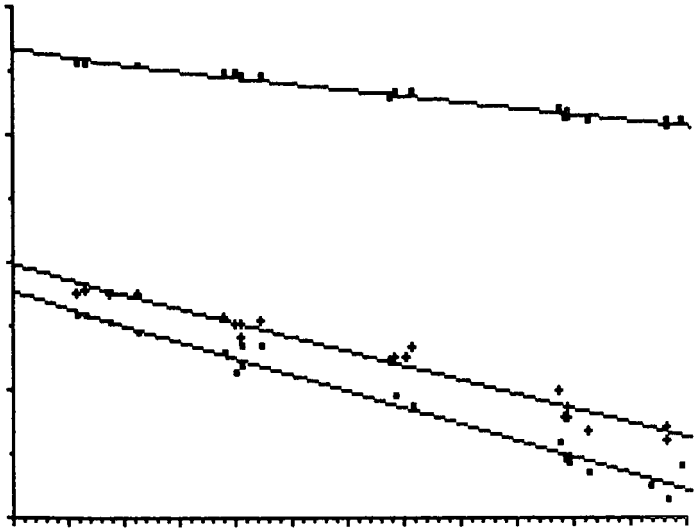

FIGURE 4. ARRHENIUS PLOT OF FLUIDITY CHARACTERISTICS OF COAL #41. Horizontal: 1000/°K, scale 1.40 to 1.46 (441-412°C). Vertical: ln(function), scale -1.5 to +2.5. From top to bottom: ln(maximum fluidity), melting slope, coking slope.

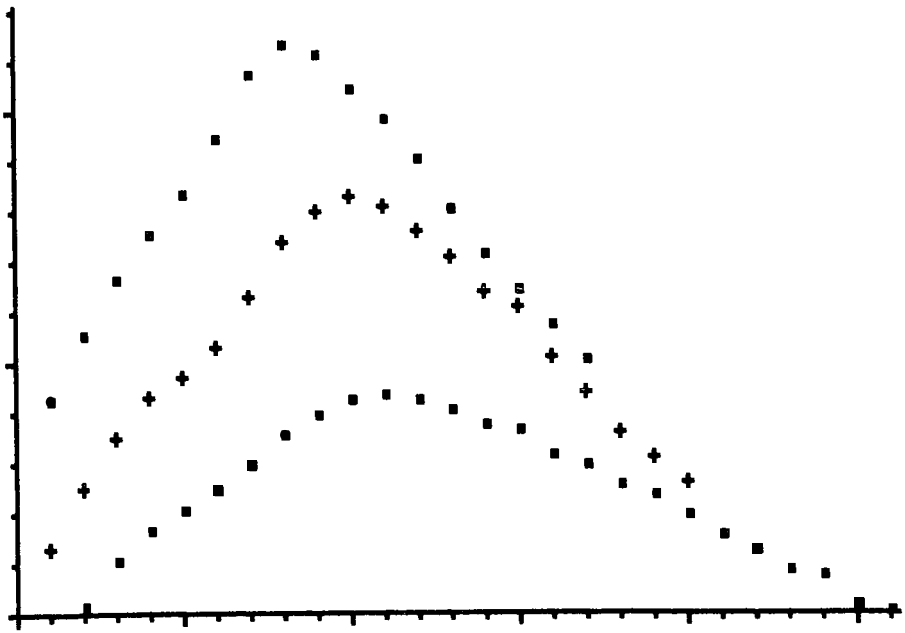

FIGURE 3. ISOTHERMAL PLASTOMETRY OF COAL #41 AT 431, 424 AND 412°C. Horizontal: time in minutes, scale 0 to 26. Vertical: ln(fluidity in ddpm), curves offset.

Predictors of Isothermal Fluid Properties of Coals

William G. Lloyd,* John W. Reasoner,* Carol L. Reagles,**
Carol P. Clark,* Jana M. Whitt,* James C. Hower,***
Linda P. Yates,*** and Eileen Davis***

*Department of Chemistry, Western Kentucky University, Bowling Green, KY 42101

**Department of Mathematics, Western Kentucky University, Bowling Green, KY 42101

***Institute for Mining and Minerals Research, University of Kentucky, Lexington, KY 40506

Fluidity, which typically develops in the range 380-420°C, is a unique property of mid-ranked coals. Coals of similar rank and composition, however, often exhibit Gieseler fluidities differing by several orders of magnitude. The objective of this study is to seek to identify predictively useful correlations between other well-defined parameters and the fluid properties of hvb coals.

In the standard Gieseler plastometer analysis (1) the coal is heated at a constant 3 deg C/min throughout the run. There are, however, several advantages to be gained by operating the plastometer in an isothermal mode, among them the more accurate determination of melting and coking slopes and the determination of the activation energies associated with these slopes and with maximum fluidities (2). In this study we use the isothermal fluid characteristics of a group of hvb coals as the dependent variables. We will examine a number of standard and nonstandard characterizations of coals for their predictive power with regard to these fluid properties.

Twenty-nine coal samples were collected from eastern mid-continent seams (mostly from western Kentucky), from active mines and from coal cleaning plants using freshly mined coal of known local origin. To minimize adventitious weathering of the samples, all coals were reduced, split and stored in sealed heavy plastic under inert gas at freezer temperatures prior to testing. The proximate, ultimate and short petrographic characterizations are given in Table 1. More detailed source information is available elsewhere (3).

For each of these coals a number of isothermal Gieseler determinations (at least 18) has been made. Both melting and coking slopes follow Arrhenius dependencies (2,4), as do ln(maximum observed fluidity) and ln(intersection maximum fluidity) (2). For direct coal-to-coal comparison it is convenient to make an interpolation or short extrapolation of temperature to a benchmark value such as 400°C. Table 2 summarizes the fluidity characteristics of these coals, with slope and fluidity data estimated for 380, 400 and 420°C. The maximum Gieseler fluidities (by slope intersection) of these coals cover a wide range, ranging at 400°C from 62,300 ddpm (coal 25) to 1.8 ddpm (coal 28).

In addition to the characterization data summarized in Table 1, several nonstandard measurements have been made. These are described below.

When small portions (3-5 mg) of coal are pyrolyzed at a high ramp (500 deg C/sec) and low ceiling temperature (450°C) onto a nonpolar chromatographic column, the resulting chromatogram provides information in two distinct regions, a gaseous product mixture which quickly elutes from a 50 cm silicone (OV 101) column at 60°C, and a larger vapor product mixture eluting at 200-250°C. A standard pyrolysis/GC procedure has been developed (5), wherein the integrator signals in several one-minute windows are found to correlate significantly with observed fluid properties. This is a reasonably reproducible procedure, with standard deviations

(quadruplicate analyses) averaging 6.5% of the total integrator signal per microgram coal.

Total organic material extractable by refluxing tetrahydrofuran (THF) and refluxing N,N-dimethylformamide (DMF) has been determined for all coals by Soxhlet extraction in triplicate. The average amount extracted by THF (dry ash-included basis) is 14.3%, average standard deviation 0.29%. The average amount extracted by DMF (same basis) is 25.1%, average standard deviation 0.85%. It is necessary to heat residues to 150°C under 1 torr in order to obtain complete desorption of the nitrogen base (6).

Two other kinds of data were obtained and found to have no predictive value with regard to plasticity. If fluid properties were related to low covalent crosslink densities, then the swelling (7,8) of DMF extraction residues by cold DMF might be expected to correlate with fluidities. Residues from four coals were swelled to equilibrium by direct contact with liquid solvent in a simple apparatus adapted from Larsen (7). The four coals had ASTM maximum fluidities ranging from 35 to over 30,000 ddpm. The swelling ratios were all between 2.1 and 2.5, with the most fluid coal having one of the lower swelling ratios. This observation seems to rule out the possibility that fluidity differences among hvb coals arise from differences in covalent crosslink densities.

The second experiment productive of negative results was that of FTIR examination of selected coals and their THF extracts, using the procedure described by Painter (9,10) and the H(aromatic)/H(aliphatic) ratio technique of Solomon (11). Two low-fluidity coals, 03 and 24, and two highly fluid coals, 22 and 34, were compared. The aromatic/aliphatic ratios are slightly different for the raw coals (0.43 and 0.45 for the low-fluidity coals and 0.47 and 0.49 for the high-fluidity coals), and are identical for the THF extracts (0.33 for all four coal extracts). This appears to rule out the view that variations in fluid behavior reflect substantial variations in the chemical characteristics of the sol fractions.

The following 'independent' variables were collected for first-round prediction testing:

16 classical characterizations, including seven petrographic measurements;

6 semistandard characterizations (ash sulfate, organic and pyritic sulfur, aliphatic/aromatic ratio, and DMF and THF extractables);

25 measures (with considerable redundancy) of the pyrolysis/GC chromatograms; and

9 sets of values derived from the above (five estimates of reactive macerals, 2 estimates of H/C ratio, an empirical formula for estimating liquefaction reactivity from % hydrogen and organic sulfur, and an estimate of extractable 'preasphaltenes' as [DMF-THF]).

These parameters were examined separately by simple linear regression, using the SAS (12) R-square test, to reduce the candidate independent variables to a manageable number. The number of variables was reduced to 13, using two criteria. A candidate variable is rejected if the fraction of the total sums of squares accounted for by a simple linear regression using the candidate variable is less than 0.1, and/or the variable is redundant with another variable which has stronger predictive power. (For example, pyritic sulfur is less predictive than total sulfur, and with total sulfur present in the analysis pyritic sulfur does not

provide sufficient additional predictivity.) The variables surviving this screening are shown in Table 3.

The best single predictor of fluidity at 400-420°C is the 4-5 min pyrolysis/GC signal (the gas signal from fast pyrolysis to 450°C), which affords correlation coefficients of .850 at 420 and .867 at 400°C. In the absence of pyrolysis/GC data the next best predictor is total DMF-extractables, affording correlation coefficients of .851 at 420 and .812 at 400°C.

The expansion of the regression equation to include additional independent variables always increases the goodness of fit. After the third variable is added, however, improvement in the correlation coefficient R becomes quite small. In predicting ln(maximum intersection fluidity) at 400°C, for instance, the values of R with the successive addition of the 4-5 min pyrolysis/GC signal, vitrinite reflectance, THF-extractables and total sulfur are .867, .895, .920 and .935. When pyrolysis data are excluded, the successive inclusion of DMF-extractables, vitrinite reflectance, THF-extractables and % resinite yields R values of .812, .856, .890 and .901. In these and other cases the improvement obtained by adding the fourth predictive variable is of marginal statistical significance. The following observations are based upon the most consistent three-variable regressions provided by this database.

When only classical and petrographic data are available the best three-term linear regressions provide fits with R in the vicinity of 0.7-0.8 (Table 4). This is illustrated by the regression plot for ln(maximum intersection fluidity) at 400°C (Figure 1). The variables used here are heating value, total sulfur, and maximum vitrinite reflectance.

With the addition of quantitative Soxhlet extraction data, a regression on the same fluidity data using vitrinite reflectance, THF-extractables and DMF-extractables provides a reasonably good fit (Figure 2), with R = .890.

With the further addition of the pyrolysis/GC data, inclusion of the 4-5 min pyrolysis signal, along with vitrinite reflectance and THF-extractables, provides a still better fit (Figure 3), with R = .920. The predictions at 420°C are comparably good (Table 4).

An important test for the adequacy of any predictive model is the examination of residuals for possible patterning. A plot of the residuals from the regression of Figure 3 is shown in Figure 4. The substantially random distribution of these residuals suggests that most of the data scatter of Figure 3 represents random error (sample inhomogeneity and errors of sampling, analysis, and possibly adventitious sample ageing during the various analyses).

Discussion.

It has not proven to be possible to predict fluid properties of coals on the basis of a single chemical or petrographic characterization. Even solvent extraction with pyridine or quinoline (13) appears to be little more than roughly indicative. In the present study DMF-extractables constitute an approximate predictor (R > 0.8), and a part of the 450° pyrolysis gas signal is a slightly better predictor.

The above data (Table 4) show reasonably good prediction (R's > 0.9) of maximum fluidity and melting and coking slopes by multiple linear regression equations using three predictive variables. The data fits are not quite as good when pyrolysis or extraction data are excluded. The correlation coefficient falls to 0.85 when both pyrolysis and extraction data are excluded (Figure 1).

The measurements with the greatest significance for our data are the 4-min. pyrolysis/GC signal (or other nearly equivalent pyrolysis data), THF-extractables, DMF-extractables, heating value and vitrinite reflectance. Increases in the values of any of the first four correlate with increasing the melting slope; increasing reflectance makes little change in melting slope but diminishes the coking slope. Increases in any of these variables correlate with increased maximum fluidity.

The relative importance of predictive variables varies with the situation. DMF-extractables is a considerably better single predictor than THF-extractables; yet in most multivariate cases THF-extractables make a larger Type IV contribution to regression sums of squares than do the DMF data. It is tentatively suggested that the DMF data are partially redundant with the pyrolysis data. We are not yet able to offer a specific mechanistic interpretation of these observations.

After examination of a number of expressions containing predictors raised to other than the first power, and a number of expressions with cross-terms containing products of two predictors, the simple first-order linear equations of Table 4 seem to be as good as any. We are continuing to apply factor analysis to these data, with the objective of characterizing more clearly the underlying physicochemical features controlling fluid behavior in coals.

This work is part of a larger study of coal plasticity, for which we acknowledge with thanks the support of the U.S. Department of Energy (3).

References

1. ASTM Method D 2639, Amer. Soc. for Testing and Materials, Phila., PA, 1982.
2. W. G. Lloyd, J. W. Reasoner, J. C. Hower and L. P. Yates, Amer. Chem. Soc., Divn. Fuel Chem., preceding paper.
3. W. G. Lloyd, J. W. Reasoner, J. C. Hower, L. P. Yates, C. P. Clark, E. Davis, A. Fitzpatrick, S. Irefin, A. Jiminez, T. McC. Jones, C. L. Reagles, L. P. Sturgeon, J. M. Whitt and G. Wild, 'Predictors of Plasticity in Bituminous Coals', Final Techn. Rept., U. S. Dept. of Energy Contract DE-FG22-81PC40793, January 1984.
4. W. G. Lloyd, H. E. Francis, M. R. Yewell, Jr., R. O. Kushida and V. D. Sankur, Amer. Chem Soc., Divn. Fuel Chem. Preprints, 25, no. 2, 128 (1980).
5. J. W. Reasoner, J. C. Hower, L. P. Yates and W. G. Lloyd, submitted to Fuel.
6. A. W. Fort (Univ. of Kentucky), private communication.
7. J. W. Larsen, 'Coal Structure and Reactivity', USDOE Contractors' Conf., Pittsburgh, PA, Oct. 1982.
8. N. A. Peppas, L. M. Lucht, M. E. Hill-Lievense and D. T. Hooker, II, 'Macromolecular Structural Changes in Bituminous Coals during Extraction and Solubilization', Final Techn. Rept., U. S. Dept. of Energy Contract DE-FG22-80PC30222, August 1983.
9. P. C. Painter, R. W. Snyder, M. Starsinic, M. M. Coleman, D. W. Kuehn and A. A. Davis, Appl. Spectroscopy, 35, 475 (1981).
10. P. C. Painter, R. W. Snyder, M. Starsinic, M. M. Coleman, D. W. Kuehn and A. A. Davis, 'Coal and Coal Products: Analytical Characterization Techniques', in E. L. Fuller, ed., ACS Symp. Ser. 205, Amer. Chem. Soc., Washington, DC, 1982.
11. P. R. Solomon, Amer. Chem. Soc., Divn. Fuel Chem. Preprints, 24, no. 3, 184 (1979).
12. Statistical Analysis System, SAS Institute, Inc., Cary, NC.
13. K. Ouchi, K. Tanimoto, M. Makube and H. Itoh, Fuel, 62, 1227 (1983).

Table 1[1]

coal	rank	moist.	ash	VM	%C	%H	%N	%S	pyrS	orgS	Btu	FSI	vit[2]	lip[3]	min[4]	refl[5]
02	hvBb	7.86	10.77	42.6	71.67	5.05	1.62	3.41	1.43	1.96	12620	4.5	66.4	7.2	13.5	0.42
03	hvBb	6.75	5.40	41.6	77.60	5.38	1.60	2.02	0.98	1.02	13720	4	85.2	5.0	7.0	0.70
04	hvBb	5.33	6.44	46.8	76.48	5.37	1.60	3.29	2.22	0.92	13650	3.5	74.4	7.6	8.8	0.59
06	hvBb	5.02	7.86	44.5	72.19	5.09	1.11	3.68	1.38	2.27	13300	6	78.4	4.2	10.5	0.57
07	hvBb	5.21	6.48	44.8	76.46	4.78	1.04	3.20	1.08	2.08	13590	3.5	81.9	2.7	8.8	0.60
09	hvBb	7.76	8.79	41.4	73.16	5.43	1.52	3.13	1.25	1.99	13050	4.5	75.4	4.2	11.6	0.58
10	hvBb	6.32	8.49	41.7	75.08	4.30	1.13	3.14	1.18	1.85	13330	4	75.5	2.8	10.9	0.57
11	hvBb	5.94	17.71	38.4	63.32	4.61	1.25	3.40	1.61	1.63	11770	2.5	69.7	3.2	21.0	0.56
14	hvBb	6.70	7.60	41.1	74.12	5.21	1.35	2.75	0.93	1.76	13410	4	79.1	3.1	9.7	0.54
15	hvBb	6.31	10.38	41.3	73.18	5.47	1.54	3.77	1.62	2.10	12850	4.5	71.7	3.7	13.3	0.61
18	hvBb	7.09	8.36	40.6	74.08	5.11	1.50	3.59	1.47	1.86	13020	4.5	77.3	3.9	11.0	0.54
20	hvBb	7.77	9.70	43.5	74.06	5.28	1.22	2.92	0.92	1.71	12910	5	79.9	2.9	11.8	0.53
21	hvAb	2.57	8.68	40.3	75.41	5.27	1.07	3.35	1.33	1.93	13540	8.5	75.5	4.3	11.2	0.71
22	hvAb	2.45	9.60	39.4	75.98	5.42	1.44	2.91	1.45	1.35	13490	8	76.0	3.7	12.0	0.73
24	hvBb	7.87	7.15	42.8	75.68	5.55	1.51	3.56	1.22	2.27	13300	4	80.2	3.2	9.7	0.60
25	hvAb	1.68	6.79	40.2	77.79	5.33	2.04	1.38	0.19	1.17	14250	7	75.7	5.7	8.1	0.87
26	hvAb	2.12	14.20	32.2	69.87	4.43	1.50	2.76	0.48	2.20	12610	7	72.2	2.7	17.3	0.87
27	hvAb	2.86	8.12	40.0	76.18	5.17	1.54	3.53	0.48	2.97	13650	7	71.1	3.6	10.7	0.76
28	hvCb	10.96	8.26	42.2	76.65	5.78	1.58	1.42	0.80	0.59	13240	2.5	69.0	7.8	9.7	0.64
30	hvBb	6.44	8.95	48.7	74.67	5.41	1.54	4.01	1.46	2.23	13010	4.5	68.4	9.6	11.9	0.58
32	hvAb	2.94	7.23	42.8	76.05	5.37	1.65	3.00	0.92	2.05	13730	5	78.5	3.1	9.5	0.65
34	hvAb	2.28	8.03	41.0	74.36	5.25	1.45	2.77	1.08	1.67	13670	6.5	80.5	3.9	10.2	0.69
35	hvBb	6.59	10.61	39.3	73.77	5.10	1.25	4.06	2.05	1.91	12775	6	77.5	2.7	13.7	0.58
36	hvBb	7.00	12.58	38.2	70.38	4.91	1.29	4.06	2.22	1.72	12470	4.5	76.2	2.5	15.8	0.58
37	hvAb	3.30	12.48	37.2	72.88	4.91	1.53	2.90	1.70	1.16	12740	4.5	75.3	2.4	15.1	0.66
38	hvBb	9.89	3.41	40.5	81.75	5.64	1.65	0.83	--	--	14170	3	76.7	8.4	3.9	0.67
39	hvBb	7.63	13.41	38.5	70.57	5.12	1.56	1.91	--	--	12530	3	72.2	7.6	15.6	0.65
40	hvBb	9.29	3.75	39.6	81.33	5.68	1.73	0.80	--	--	14150	2.5	80.1	7.9	4.6	0.70
41	hvBb	7.78	2.77	42.1	80.73	5.74	1.61	1.06	--	--	14280	3	85.7	7.2	3.3	0.67

[1] Moisture is as determined; other analyses are on a dry ash-included basis. [2] Vitrinite and pseudovitrinite. [3] Exinite and resinite. [4] Mineral matter content by Parr procedure. [5] Vitrinite maximum reflectance in oil at 546 nm.

Table 2

coal	exptl T range, °C	melting slope, min^{-1} @380°	@400°	@420°	coking slope, min^{-1} @380°	@400°	@420°	ln(max observed fluidity) @380°	@400°	@420°	E(a)[1]	ln(max intersection flu) @380°	@400°	@420°	E(a)[1]
25	404-420°	0.246	0.631	1.535	.0379	.105	.276	9.52	9.93	10.34	2.	11.10	11.04	10.99	0.
34	390-409	0.371	1.232	3.823	.0653	.174	.436	8.24	9.74	11.40	7.	7.60	10.10	13.19	12.
32	389-411	0.392	1.187	3.373	.0797	.206	.506	5.56	8.40	12.39	18.	6.92	9.23	12.11	13.
27	379-404	0.197	0.875	3.564	.0565	.153	.391	4.37	8.43	15.65	29.	5.64	8.81	13.40	20.
21	387-410	0.340	1.023	2.885	.0567	.179	.526	4.84	8.11	13.19	23.	5.91	8.68	12.46	17.
22	389-413	0.193	0.702	2.375	.0429	.131	.374	4.05	6.71	10.78	22.	4.96	7.84	12.07	20.
35	400-419	0.263	0.656	1.551	.0912	.245	.624	3.63	5.87	9.21	21.	4.36	6.49	9.46	17.
06	393-418	0.156	0.518	1.606	.0620	.205	.634	2.96	5.67	10.47	28.	3.59	6.11	10.09	23.
07	404-426	0.219	0.505	1.109	.0614	.206	.645	2.58	4.43	7.36	24.	3.36	5.15	7.69	19.
37	406-432	0.179	0.431	0.986	.0648	.195	.549	1.98	3.40	5.62	24.	2.72	4.23	6.42	19.
36	404-425	0.140	0.382	0.982	.0829	.240	.656	2.00	3.46	5.79	24.	2.53	4.11	6.49	21.
14	398-422	0.215	0.466	0.966	.0942	.273	.745	1.61	3.03	5.48	28.	2.42	3.88	6.04	21.
15	400-427	0.137	0.350	0.844	.102	.276	.706	2.10	3.47	5.56	22.	2.26	3.78	6.13	22.
41	412-438	0.088	0.240	0.616	.0435	.141	.429	1.95	3.20	5.10	22.	2.35	3.68	5.63	20.
04	406-431	0.070	0.252	0.842	.0475	.168	.554	1.33	2.84	5.80	33.	2.04	3.66	6.33	26.
39	410-435	0.101	0.267	0.667	.0565	.167	.460	1.74	3.03	5.11	24.	2.04	3.43	5.58	23.
26	412-436	0.113	0.280	0.661	.0363	.109	.304	1.18	2.23	4.07	28.	1.92	3.11	4.89	21.
38	411-436	0.044	0.155	0.505	.0341	.119	.385	1.49	2.70	4.75	26.	1.73	3.07	5.26	25.
40	417-443	0.278	0.424	0.631	.0587	.161	.418	0.476	1.09	2.37	36.	1.99	2.89	4.11	16.
20	401-428	0.221	0.420	0.769	.0993	.272	.704	0.616	1.61	3.97	42.	1.42	2.67	4.85	28.
10	405-429	0.222	0.442	0.846	.0588	.214	.723	0.651	1.57	3.61	39.	1.18	2.38	4.62	31.
30	399-426	0.191	0.400	0.803	.0965	.267	.694	0.287	0.967	3.03	53.	1.01	2.12	4.26	32.
18	398-424	0.195	0.396	0.773	.0889	.270	.767	0.428	1.26	3.47	47.	0.907	2.06	4.47	36.
24	405-431	0.282	0.435	0.653	.109	.284	.701	0.394	0.916	2.03	37.	1.02	1.76	2.94	24.
11	412-432	0.286	0.493	0.824	.0486	.179	.611	0.631	1.28	2.48	31.	0.856	1.75	3.42	31.
09	403-427	0.174	0.352	0.683	.0592	.207	.671	0.252	0.813	2.45	51.	0.484	1.34	3.48	44.
03	408-433	0.092	0.235	0.569	.0368	.136	.467	0.273	0.704	1.72	41.	0.445	1.14	2.76	41.
02	406-423	0.176	0.316	0.546	.0611	.221	.739	0.380	0.852	1.82	35.	0.408	1.04	2.50	41.
28	413-437	0.201	0.394	0.743	.0123	.0670	.329	0.160	0.339	0.687	33.	0.314	0.585	1.05	27.

[1] Activation energy in kcal. The average standard deviation of E(a) of 1.9 kcal.

Table 3

Variables Retained for Multiple Linear Regression Analysis

Class:		R^2 in simple regression*
Classical	FSI	.260
	BTU	.122
	% Sulfur	.031[1]
Petrographic	Exinite	.128
	Resinite	.105
	Pseudovitrinite	.290
	Max Vitrinite Reflectance	.246
Extraction	DMF-extractables	.554
	THF-extractables	.199
Pyrolysis/GC	4-5 min signal %[2]	.595
	2-5 min signal counts[2]	.572
	14-16 min signal counts[3]	.572
	13-17 min window counts[3]	.565

* Averages for six estimates: max observed fluidity at 400° and 420°, and E(act), and max intersection fluidity at 400° and 420°, and E(act).

[1] Retained owing to good predictive power for coking slopes.
[2] The 4-5 min signal % and 2-5 min signal counts are substantially redundant.
[3] The 14-16 min and 13-17 min signal counts are substantially redundant.

Table 4

Best-fit Three-value Multiple Linear Regression Equations

Equation[1]	Corr. coeff.
CLASSICAL AND PETROGRAPHIC DATA ONLY:	
MELT400 = -1.128 +1.309E-4 * BTU -8.857E-2 * EXIN +2.531E-1 * RESI	.785
MELT420 = -5.986 +5.793E-4 * BTU -2.758E-1 * EXIN +6.919E-1 * RESI	.692
COKE400 = +0.078 +1.582E-5 * BTU +3.356E-2 * SULF -3.018E-1 * REFL	.806[2]
COKE420 = +0.757 +2.401E-5 * BTU +6.273E-2 * SULF -1.103EØ * REFL	.913[2]
FCAL400 = -44.32 +2.419E-3 * BTU +1.815EØ * SULF +1.789E+1 * REFL	.721
FCAL420 = -54.54 +3.101E-3 * BTU +2.643EØ * SULF +1.962E+1 * REFL	.723
WITH EXTRACTION AND PYROLYSIS/GC DATA AVAILABLE:	
MELT400 = -0.311 +1.224E-1 * RESI +3.168E-2 * THF +3.287E-1 * PYR4	.906
MELT420 = -1.369 +2.388E-1 * RESI +1.025E-1 * THF +1.285EØ * PYR4	.904
FCAL400 = -9.998 +1.102E+1 * REFL +3.374E-1 * THF +3.369EØ * PYR4	.920
FCAL420 = -11.59 +1.134E+1 * REFL +5.767E-1 * THF +3.731EØ * PYR4	.912

[1] Abbreviations: MELT400 and MELT420 - melting slopes at 400° and 420°C; COKE400 and COKE420 - coking slopes at 400° and 420°C; FCAL400 and FCAL420 - ln(intersection maximum fluidity) at 400° and 420°C; BTU - heating value; EXI - % exinite; REFL - % maximum vitrinite reflectance; RESI - % resinite; SULF - % sulfur; THF - % extractable by THF. [2] Best three-variable fit.

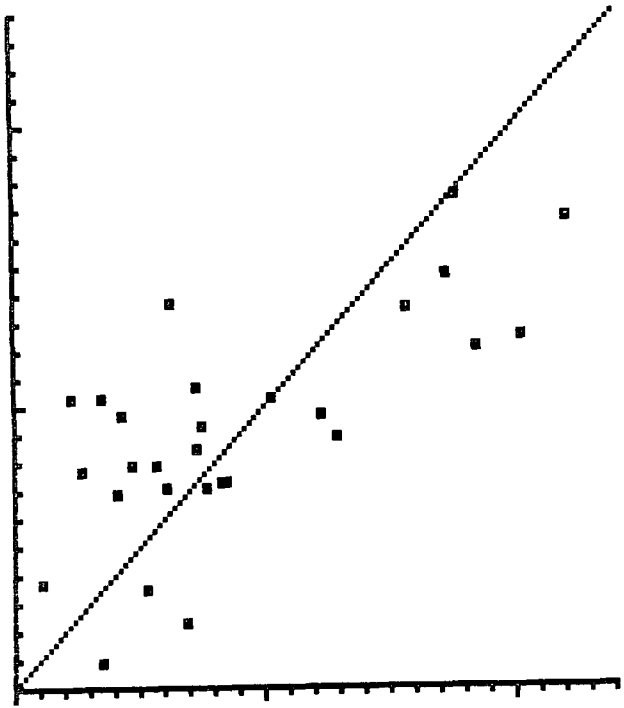

FIGURE 1. PREDICTION OF LN(MAXIMUM FLUIDITY) AT 400°C, EXCLUDING EXTRACTION AND PYROLYSIS DATA. Horizontal: ln(observed ddpm). Vertical: ln(predicted ddpm). Both scales 0 to 12. Independent variables: heating value, total sulfur, maximum vitrinite reflectance. R^2 = .520 (29 coals).

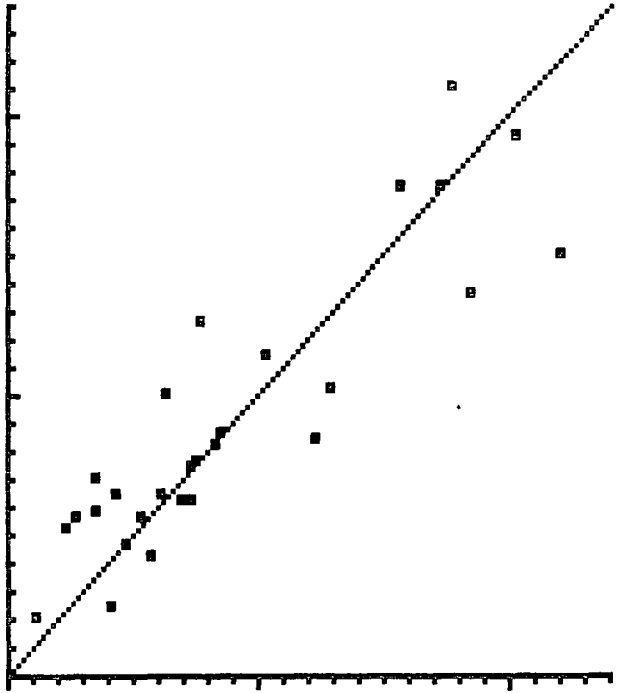

FIGURE 2. PREDICTION OF LN(MAXIMUM FLUIDITY) AT 400°C, INCLUDING EXTRACTION DATA. Horizontal: ln(observed ddpm). Vertical: ln(predicted ddpm). Both scales 0 to 12. Independent variables: maximum vitrinite reflectance, DMF-extractables, THF-extractables. R^2 = .792 (29 coals).

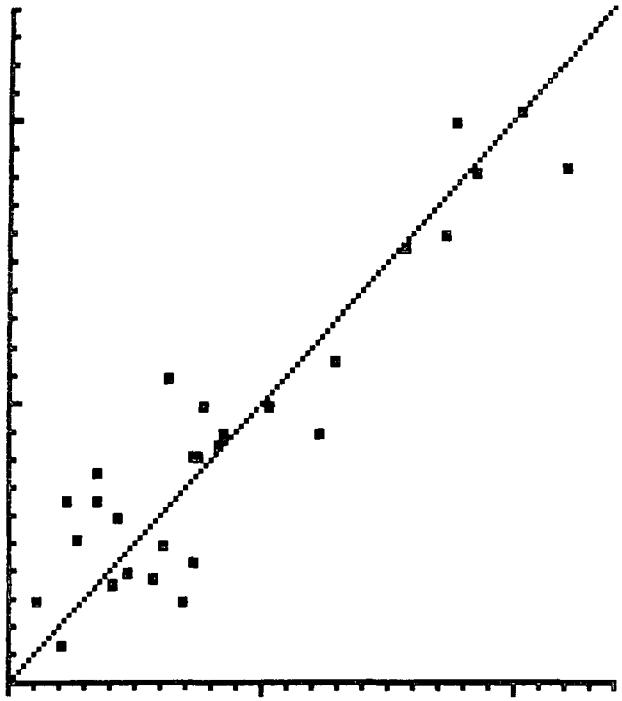

FIGURE 3. PREDICTION OF LN(MAXIMUM FLUIDITY) AT 400°C, INCLUDING PYROLYSIS DATA. Horizontal: ln(observed ddpm). Vertical: ln(predicted ddpm). Both scales 0 to 12. Independent variables: maximum vitrinite reflectance, THF-extractables, 4-5 min pyrolysis/GC signal. R^2 = .847 (29 coals).

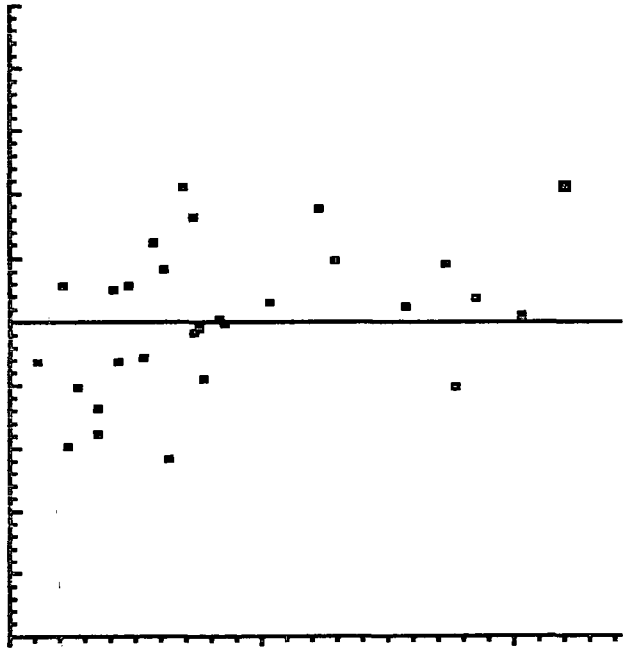

FIGURE 4. ANALYSIS OF RESIDUALS IN THE REGRESSION OF FIGURE 3. Horizontal: ln(observed fluidity, ddpm), scale 0 to 12. Vertical: residuals from regression [observed - predicted], scale -5 to +5.

VISCOELASTIC PROPERTIES OF BITUMINOUS COALS

John M. Howell and Nikolaos A. Peppas[1]

School of Chemical Engineering
Purdue University
West Lafayette, Indiana 47907

INTRODUCTION

The study of the swelling and thermal behavior of coals and the implications these have on possible coal structures are of increasing interest as industrial processes are developed for coal utilization (liquifaction and gasification). Developing accurate structural models and appropriate relations to predict the swelling and thermal behavior of coals would greatly aid plant design by enabling engineers to estimate reaction kinetics and mechanisms for reactions.

It is useful to consider coal as a crosslinked macromolecular network when explaining its swelling and thermal behavior. A crosslinked structure such as that illustrated in Figure 1 has been proposed by Lucht and Peppas [1]. This type of model is in agreement with current experimental findings and is applied in the analysis of experimental results.

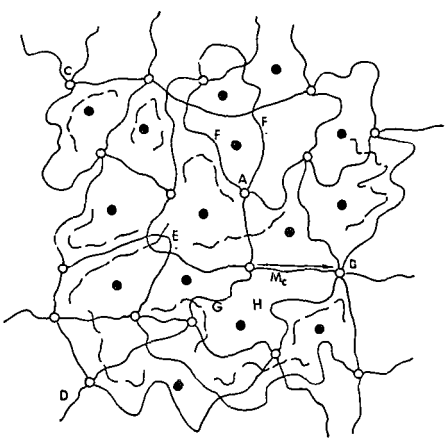

Figure 1. Simplified representation of the crosslinked structure of coal including possible defects. ——: Chains participating in network structure; — — —: extractable (unreacted or degraded) chains; O : crosslinks (junctions); ● molecules of swelling agent; $\bar{M}_c$: molecular weight between crosslinks; A: tetra-functional crosslink; B: multifunctional crosslink; C: unreacted functionalities; D: chain end; E: entanglement; F: chain loop; G: effective network chain; H: mesh size.

Chemical and Physical Structure of Coal

Interpreting the physical structure of macromolecular chains in coal with cross-linked macromolecular network models and theories has become increasingly common in the recent past, although such models have existed for over twenty years [2]. If mineral matter, ash and other impurities naturally occuring in coal are excluded,

---

1. Corresponding author

coal structures can be described by two distinct phases. The first phase consists of small and large molecules which are uncrosslinked and occupy a substantial portion of the whole coal sample. These macromolecular chains can be intact uncrosslinked molecules formed during diagenesis [3], or somewhat degraded chains formed by depolymerization reactions during the metamorphic stage of coal development. The primary phase of the coal structure consists of a highly crosslinked macromolecular phase forming a crosslinked three-dimensional network (coal matrix) [1]. This is the structure shown in Figure 1, which depicts several forms of macromolecular chains and possible chain defects.

The crosslinked structure cannot be extracted or dissolved at low temperatures (unless the solvent acts by combined diffusion and reaction, as in depolymerization), and is characterized by both physical and chemical crosslinks. Physical crosslinks are found in highly entangled macromolecular chains that, because of inherent rigidity, have restricted mobility. In this case, disentanglement is not likely. Chemical crosslinks are formed by chemical reactions between two or more coal chains, which lead to multifunctional crosslinks.

Coal researchers have considered models of various "reconstructed" chemical structures of coal as a means to support their theories [3]. But model networks such as those proposed by Wiser and Given are only indicative of the type of chemical crosslinks one would expect in coal, and are not proof of the physical structure of coal or the size of macromolecular chains between crosslinks. Chain ends, unreacted functionalities, chain loops and multifunctional crosslinks are types of defects which make an accurate analysis of the coal network unlikely.

The nature of the crosslinks in coal is a point of scientific dispute. Most of the work on identifying coal crosslinks relies on analysis of the products of depolymerization and degradation reactions. Because the system is complex and strong intermolecular interactions occur, analyzing the results is difficult, often leading only to speculations about chemical structure [3,4].

A promising analytical technique for degradation products (coal liquids) is based on mass-analyzed ion kinetic energy spectrometry. Other techniques have been used including elemental analysis and identification of decomposition and extraction products from coal, IR spectroscopy, high resolution NMR, and GC/mass spectroscopy. These results have given us a clearer understanding of the types of chemical bonds involved in crosslinking.

Viscoelastic Properties of Coal

One aspect of the macromolecular coal structure which has been given very little attention upto now is its viscoelastic behavior. It is in general known that coal at high temperatures, close to the liquefaction temperature of 300-350°C, softens and behaves as a highly viscous material. Its viscosity becomes dependent on the conditions of application of stress or strain. For example, Nazem [5] studied the non-Newtonian behavior of carbonaceous mesophase pitch at high temperatures using a Haake viscometer and established the non-Newtonian behavior in terms of the viscosity as a function of the shear rate. Briggs [6] investigated the viscosity of coal tar pitch as a function of temperature. Covey and Stanmore [7] attempted to present a constitutive equation for the rheological behavior of Victorian brown coals of Australia.

An alternative approach of investigation of the viscoelastic behavior of coals is through thermal analysis at high temperatures. The early work of Bangham and Franklin [8] established characteristics of the change and expansion of the coal structure at high temperatures. More recently Sanada and Honda [9] used creep deformation experiments of various Japanese coals to establish their mechanical behavior at high temperatures. Finally, Rovenskii and Melnik [10] were the first and probably the only investigators upto now to investigate the use of thermomechanical analysis as a method of characterization of coals.

Here we present new and important information on the results of thermomechanical analysis of some American bituminous coals.

EXPERIMENTAL PART

Previously stored in nitrogen, flat coal samples of the following coals were used in the present studies: PSOC-418 (69.95% C, dmmf basis), PSOC-791 (72.75% C), PSOC-312 (78.33% C), PSOC-853 (80.15% C), PSOC-402 (82.48% C) and PSOC-989 (88.81% C); all obtained from the coal bank of the Pennsylvania State University. All samples had an initial surface area of approximately 2.5 mm^2. They were tested in a thermomechanical analyzer (model TMS-2, Perkin Elmer, Norwalk, Conn.) using the penetration mode of the device, under continuous purging of nitrogen and starting from an initial temperature of 35°C. The tip of the probe was round with a surface area of 0.6207 mm^2. All samples were tested under the application of loads of 10, 20, 30 and 40 g corresponding to stresses of 0.158, 0.316, 0.474 and 0.632 MPa, respectively. Unless otherwise noted, all studies were performed at a scanning speed of 10°C/min and upto 350°C. The deformation was determined as a function of time and transform to strain by dividing by the original thickness of the flat samples.

RESULTS AND DISCUSSION

Figures 2 and 3 present the strain versus time curves for two of the samples tested, a PSOC-791 sample with 72.75% C on a dmmf basis and a PSOC-312 sample with 78.33% C. It must be remembered that, since the scanning speed is 10°C/min, the same plots represent the deformation, as designated by the strain, as a function of temperature.

All curves show an early induction period which lasts for approximately 5-10 minutes or 50-100 °C and is characteristic of the very slow compressive creep of highly glassy polymeric materials. Indeed for these coals we have determined [11] values of Tg in the range of 300-350°C, much higher than the temperatures at the beginning of these experiments. After about 18 to 25 minutes from the beginning of the experiment, corresponding to temperatures of 215°C to 285°C, a plateau is observed in the strain versus time behavior. Further temperature increase leads to considerable increase of the strain probably due, either to yielding of the macromolecular coal structure at temperatures where enough mobility of the macromolecular chains has been attained, or to thermal degradation at these temperatures. However, the second explanation is probably not valid since thermogravimetric

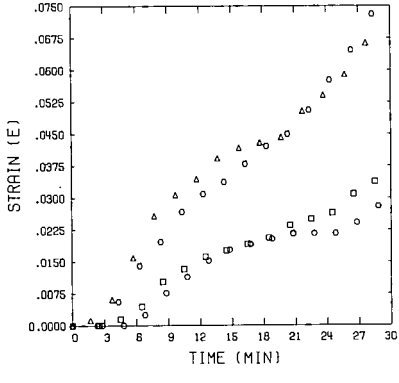

Figure 2: Compressive strain as a function of time for flat coal samples of PSOC-791 (72.75% C, dmmf basis). The results are for applied stresses of 0.158 (O), 0.316 (□), 0.47 (Δ) and 0.632 (O) MPa.

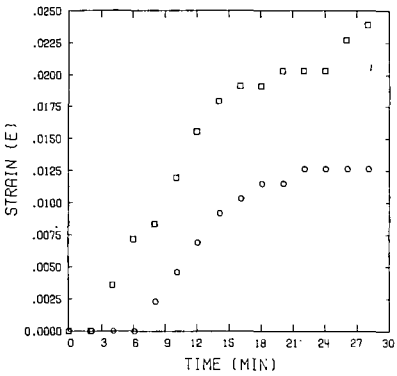

Figure 3: Compressive strain as a function of time for flat coal samples of PSOC-312 (78.33% C). The results are for applied stresses of 0.474 (o) and 0.632 (□) MPa.

analysis experiments under the same scanning speed using a thermogravimetric analyzer (TGS-2, Perkin Elmer, Norwalk, Conn.) showed little measurable weight change of the coal samples up to 250°C.

Figure 2 shows also the general dependence of the strain on stress. Indeed, as the stress increases, the strain is higher and the point of deviation from the original plateau is at lower temperatures (or times), which is characteristic and typical of similar behavior in polymer networks.

Finally, comparison of the data of Figures 2 and 3 at the same stress shows that for the coal samples with the lower carbon content, at the same scanning time the strain is much higher than that of the samples with higher carbon content. This is a clear indication that PSOC-791 is less crosslinked than PSOC-312, a notion which is clearly supported by our recent data on the determination of $\bar{M}_c$ of these and other coals [12]. Samples PSOC-402 (with 82.48% C) and PSOC-989 (with 88.81% C) were tested not only at these stresses but also at 0.790 and 0.948 MPa. In no cases was any deformation observed, an observation characteristic of very highly crosslinked structures.

Further analysis of these data was achieved by using the Nutting theory, which when applied to creep data, suggests that the creep compliance is logarithmically dependent on time according to equation (1).

$$J = \psi t^n \qquad (1)$$

Here J is the coal structure compliance, which is calculated from the previous graphs by dividing the strain by the applied stress, t is the creep time and ψ and n are two constants characteristic of the coal structure.

Figure 4 shows a plot of ln J versus ln t for the samples of PSOC-791 plotted earlier. Although one would expect a linear relationship between these two parameters there are some important deviations. For example, the initial portion of the graph, characteristic of the slowly changing induction period could not be represented by the Nutting equation, because of the highly "frozen" structure of the macromolecular network of coal. The region between ln t of 2 and 3.2 can be reasonably represented by straight lines, which in accordance with Nutting's equation, are parallel for different stresses.

An interesting aspect of these studies is also shown in Figure 5 which presents the insignificant effect of the scanning speed rate on the strain-time behavior. The same figure shows that a continuous increase of the strain is observed even

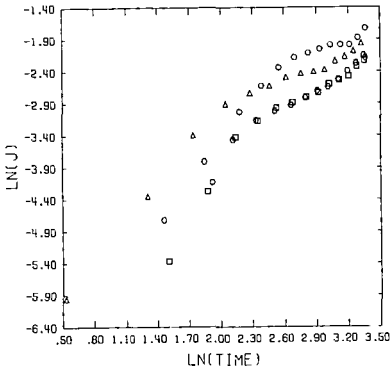

Figure 4: Nutting plot of the compliance of coal structures as a function of time for PSOC-791 (72.75% C). The data are for the same stresses as in Figure 2.

after 60 minutes (at 5°C/min), corresponding to a temperature of 335°C, where the coal "flows" since it is above its Tg.

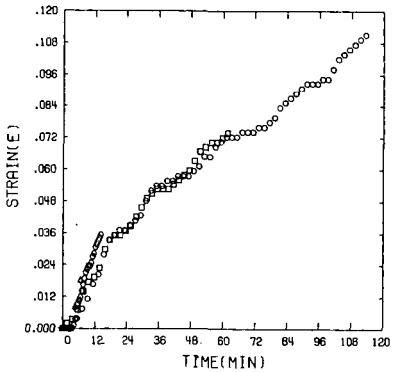

Figure 5: Effect of scanning speed on the strain-time curve. Results for coal PSOC-418 (69.95% C) with 2.5 (○), 5(□), 10 (△) and 20 (⬡) °C/min.

CONCLUSIONS

These results further support the idea of a highly crosslinked, macromolecular coal network [1], and are indicative of the difficulty by which the thermal degradation occurs.

Aknowledgements

This work was supported by research grant DOE-F6-22-83PC60792 of the Department of Energy, Pittsburgh Energy Technology Center. Helpful discussions with Dr. L.M. Lucht are kindly acknowledged.

REFERENCES

1. L.M. Lucht and N.A. Peppas, in B.R. Cooper and L. Petrakis, eds., "Chemistry

and Physics of Coal Utilization," 28, American Institute of Physics, New York, N.Y. 1981.
2. L. Lazarov and G. Angelova, Khim. Tverd. Topl., 10(3), 15 (1976).
3. N. Berkowitz, "An Introduction to Coal Technology," Academic Press, New York, Y.Y., 1979.
4. J.W. Larsen and E.W. Keummerle, Fuel, 55, 162 (1976).
5. F.F. Nazem, Fuel, 59, 851 (1980).
6. D.K.H. Briggs, Fuel, 59, 201 (1980).
7. G.H. Covey and B.R. Stanmore, Fuel, 59, 124 (1980).
8. D.H. Bangham and R.E. Franklin, Trans. Faraday Soc., 42B, 289 (1946).
9. Y. Sanada and H. Honda, Fuel, 42, 479 (1963).
10. V.I. Rovenskii and N.P. Mel'nik, Khim. Tverd. Topl., 9(4), 36 (1975).
11. L.M. Lucht, J.M. Larson and N.A. Peppas, Bull. Amer. Phys. Soc., 28, 566 (1983).
12. L.M. Lucht, Ph.D. Thesis, School of Chemical Engineering, Purdue University, 1983.

THE MOLECULAR WEIGHT BETWEEN CROSSLINKS OF SELECTED AMERICAN COALS

Lucy M. Lucht[1] and Nikolaos A. Peppas[2]

School of Chemical Engineering
Purdue University
West Lafayette, Indiana 47907

INTRODUCTION

Van Krevelen (1961) and Sanada and Honda (1966, 1967) were the first to propose that the organic portion of bituminous coals can be considered as a "crosslinked polymer" (sic). Since then, Larsen and Kovac (1978), and Lucht and Peppas (1981a) have developed mathematical, topological, and physicochemical models which describe network structure of coals by accurate and physically complete theories.

Lucht and Peppas (1981a) proposed that the organic phase of coal consists of a crosslinked macromolecular structure which does not dissolve at low temperatures unless reaction and degradation occur; and of a portion of uncrosslinked macromolecular chains of predominately aliphatic character, which can be extracted at low or moderate temperatures if an appropriate solvent is used. These uncrosslinked molecules may be material from the original matter formed during diagenesis, or partially degraded chains that were formed through depplymerization reactions during the development of coal. Figure 1 shows a simplified description of the organic phase according to Lucht and Peppas. The same scheme includes not only ideal chemical crosslinks (A,B) but also unreacted functionalities (C), chain ends (D), and various defects of the macromolecular structure such as loops (F) and physical crosslinks (E), known as entanglements. Physical crosslinks occur because the system is highly entangled, that is the chains are rigid and have limited mobility. Hence, they are unlikely to disentangle when stressed or swelled. Chemical crosslinks are formed by chemical reaction of two or more chains to yield a multifunctional crosslink.

The chemical nature of the corsslinks found in coal has not been adequately determined. In the development of mathematical models to describe the behavior of the network, crosslinks are assumed to be points or short bridges with a molecular weight much smaller than $\overline{M}_c$. Here $\overline{M}_c$ refers to the statistical number average molecular weight between crosslinks of the coal structure. Obviously, as $\overline{M}_c$ increases the degree of crosslinking decreases.

To further simplify the macromolecular structure in order to make it tractable for statistical analysis, Lucht and Peppas (1981b) proposed a crosslinked coal structure, where the crosslinks are bonding regions similar to groups proposed by Wiser (1977) (see Figure 2). Each chain consists of groups of aromatic clusters and connecting bonds. The cluster may be a structure of two or more aromatic or heterocyclic rings fused together, whereas the connecting bonds are simple groups such as -O-, -S-S- and $-CH_2-$. In addition, the macromolecular chains which constitute a large portion of the coal do not exhibit a repeating unit, as defined in conventional polymers. Thus, coal does not have a "polymer structure" but a *macromolecular structure*.

The unfortunate use of the term "polymeric structure" by Van Krevelen (1961), has created some confusion, not only among coal scientists, who try to analyze the crosslinked structure, but also among polymer scientists, who try to apply statistical mechanical theories. A hypothetical repeating unit may be defined, solely for purposes of application of topological, statistical mechanical, and swelling theories, for the determination of $\overline{M}_c$.

Experimental techniques which support the existence of a crosslinked structure are based on extraction and swelling of the coal sample or coal matrix with thermodynamically "good" solvents such as pyridine and ethylene diamine, and thermodynamically

1. Present address: Lawrence Livermore Laboratory, P.O. Box 808, Livermore, CA 94550.
2. Corresponding author.

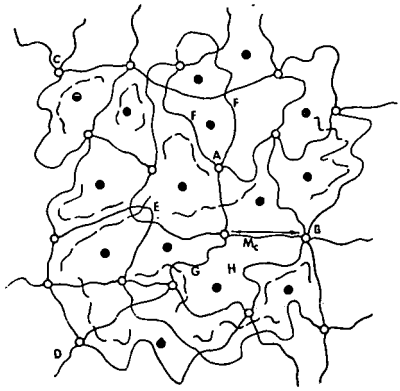

Figure 1. Simplified Representation of the Crosslinked Structure of Coal Including Possible Defects. ____: Chains participating in network structure; ----: extractable (unreacted or degraded) chains; o: crosslinks (junctions); •: molecules of swelling agent; $\overline{M}_c$: molecular weight between crosslinks; A: tetrafunctional crosslink; B: multifunctional crosslink; C: unreacted functionalites; D: chain end; E: entanglement; F: chain loop; G. effective network chain; H: mesh size.

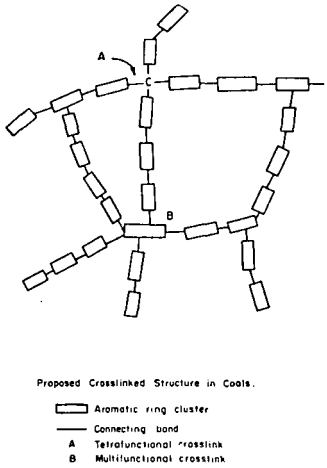

Figure 2. Proposed Crosslinked Structure in Coals According to Lucht and Peppas (1981).

"poor" solvents such as methanol, benzene, ethanol, etc. Most of the studies have been performed using either Soxhlet extraction, or simple or sophisticated dynamic swelling experiments. The term "solvent" is used here interchangeably to describe liquids which dissolve coal, and also liquids which swell it or react with it.

Here we present recent experimental results which characterize the organic phase of coal in terms of parameters of the crosslinked structure.

EXPERIMENTAL PART

Coal samples which had been ground to an average particle size of 20-30 mesh (600-850 μm) and packed under nitrogen were furnished by the coal bank of Pennsylvania State University.

Extraction was used to separate the coal matrix from material which is free or loosely held in the interstices. In a typical extraction, a coal sample of 20-30 mesh particle size and approximately 3 g. was weighed to ± 0.0001 g, and extracted in a Soxhlet apparatus using pyridine (Aldrich) under nitrogen at 115.5°C. The extract solution was replaced every one to four days with fresh pyridine until the extract solution appeared to be pure pyridine (usually one to eight weeks). The extracted residue was dried to constant weight under vacuum at *ca* 60°C and *ca* 0.93 MPa under flowing nitrogen.

Equilibrium swelling studies were conducted to provide the final values of the equilibrium volume fraction of coal in a solvent-swelled system at a specified swelling temperature. Data were collected via gravimetric sorption studies. Samples were dried at 60° to 80°C under flowing nitrogen at slightly greater than atmospheric pressure for at least 24 hours to remove free surface water. Preweighed samples were exposed to an environment saturated with vapors of pyridine in dessicators at specified temperatures, maintained constant either with a water bath or with a convection oven. The time required for swelling equilibrium was between 5-12 weeks. At the end of the swelling period, the samples were removed and reweighed.

RESULTS AND DISCUSSION

Equilibrium swelling studies provide the final values of the equilibrium volume fraction of coal in a solvent- swelled system, υ_2, at a specified swelling temperature. The degree of swelling, $Q = 1/\upsilon_2$, is an indicator of both solvent/coal thermodynamic interactions and of the physicochemical structures of coal. It can be used in any Gaussian or modified Gaussian network equation such as equation (1) to determine $\overline{M}_c$ and other crosslinking parameters. In addition, results can be used to quantify favorable thermodynamic interactions with a solvent for liquefaction purposes.

$$\frac{1}{\overline{M}_c} = \frac{\frac{\overline{\upsilon}}{V_1}[\ln(1 - \upsilon_2) + \upsilon_2 + \chi\upsilon_2^2][1 - \frac{1}{N}\upsilon_2^{2/3}]^3}{[\frac{1}{2}\upsilon_2 - \upsilon_2^{1/3}][1 + \frac{1}{N}\upsilon_2^{1/3}]^2} \qquad (1)$$

Here, $\overline{M}_c$ is the number average molecular weight between crosslinks; $\overline{\upsilon}$ is the specific volume of the macromolecule; V_1 is the molar volume of the swelling agent; υ_2 is the volume fraction of the macromolecule in the swollen system; χ is the Flory-Huggins thermodynamic interaction parameter; and N is the number of bond vectors in a single chain, given by equation (2) where M_r is the molecular weight of the characteristic repeating unit.

$$N = \frac{\overline{M}_c}{M_r} \qquad (2)$$

Equation (1) was developed specifically for application to the equilibrium solvent swelling of coals. This approach accounts for the finite expansion of solvent-swelled coals by limiting the extensibility of the individual chain. It is therefore more appropriate for determination of the molecular weight between cross-links, $\overline{M}_c$, via solvent-swelling studies, than the Flory-Rehner equation, which assumes that the end-to-end distance between chain ends is much less than the contour length of the chain and thus allows a chain to be infinitely extensible.

It must be noted that in our proposed model (Figure 2), a repeating unit consists

of a cluster and a connecting bond. This is a reasonable assumption in view of the comparatively small size of the connecting bond (usually $-CH_2-$, -S-S-, or -O-) with respect to the cluster size. The molecular weight of a repeating unit is about 130 for lignites, 170 for bituminous coals up to 86%C (dmmf), and 370 for coals with a higher carbon content.

Pyridine was used as the probe for most experiments because it is one of the few solvents which causes significant swelling in all but the highest rank coals; some researchers (e.g., Marzec *et al.*, 1979) believe that pyridine has a stronger interaction with coal than the extractables and that pyridine may be able to destroy hydrogen-bonding in the coal structure.

Figure 3 is a typical graph of results showing the dependence of the degree of swelling, Q, corrected for mineral matter on carbon content (on a dmmf basis). It was assumed that the organic vapor does not swell clays or metals to a significiant degree, so their weight was subtracted from the total. Pyridine vapor swelling was conducted at 35.0 ± 0.5°C for 60 days to swelling equilibrium and compared with the data obtained, as described above, over 51 days at 60 ± 0.5°C. The degree of swelling is significantly greater at 60°C than at 35°C, although the shapes of the curves are similar. At 35°C, the degree of swelling is constant at Q = 1.8-2.0 from *ca* 70%C and up to approximately 86%C, dropping as in the higher temperature case to Q = 1.1 at 91%C.

Experimental data were also obtained which show the effect of pyridine pretreatments on the solvent vapor swelling of coals. Equilibrium swelling of these samples was performed at 60 ± 0.5°C for 51 days and these data are shown in Figure 4. The shape of the curve is similar to that of the unextracted coals swelled by pyridine as shown in Figure 3, although the magnitude of the degree of swelling in the pyridine extracted coals over the carbon content range of 69.94 to 82.48%C (dmmf) is somewhat lower than for the unextracted coals, ranging from Q = 2.2 to 2.5 for the pyridine extracted coal samples as compared to Q = 2.5 to 2.8 for the untreated coal samples.

ANALYSIS

The modified Gaussian network equation (1) can be applied only to the results of swelling of coal networks which are free of uncrosslinked material, i.e., extractable material. Thus, only the results from the equilibrium swelling of pyridine-extracted coal samples were used in the determination of the molecular weight between crosslinks.

In the determination of the molecular weight between crosslinks, the volume fraction of coal in the pyridine swollen system, $\upsilon_2 = 1/Q$, was calculated on a mineral matter free basis, assuming that pores with diameter of greater than 50 Å contained condensed solvent only which did not contribute to swelling. The values of these pore volumes were determined by mercury porosimetry.

The average values of the molecular weight of a hypothetical repeating unit of coal were taken to be 130 for lignite or sub-bituminous coal samples, 170 for bituminous coal samples with carbon contents up to *ca* 86%C (dmmf), and 370 for all coal samples of rank greater than medium volatile bituminous up to semi-anthracite samples. These values were determined from the present view of the size of the aromatic/hydroaromatic clusters and their crosslinks.

The values of the thermodynamic interaction parameter, χ, for coals with carbon contents of 75.9, 82.4, and 88.2%C (dmmf) were determined by the Hildebrand-Skatchard regular solution theory from the solubility parameters determined by Kirov *et al.*, (1967). The values of the solubility parameter reported in that study were determined at 25°C, while the equilibrium swelling experiments of our work were carried out at 35, 60 and 80°C. Therefore, corrections in the solubility parameter values were made for different temperatures in the following way.

The dependence of the effective number of repeating units between crosslinks, N, on carbon content is shown in Figure 5 while the dependence of the effective molecular weight between crosslinks, $\overline{M}_c$, on carbon content is shown in Figure 6. Results from equilibrium swelling by pyridine vapor at 35°C of pyridine extracted coals were used in the application of equation (1).

The number of repeating units between crosslinks is relatively constant, ranging from N = 7.0 to 8.5, over the carbon content range of 69.96 to 82.48%C (dmmf). At a carbon content of 86.01%C (dmmf), the value of N drops to 4.6 and continues to decline

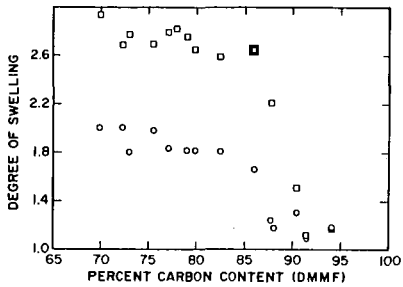

Figure 3. Equilibrium Swelling by Pyridine Vapor of 20-30 mesh, Untreated Coal Particles. (□) 60°C; (o) 35°C.

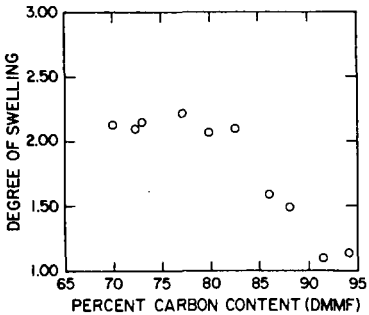

Figure 4. Equilibrium Swelling by Pyridine Vapor of 20-30 mesh, Pyridine-Extracted Coal Particles at 60°C.

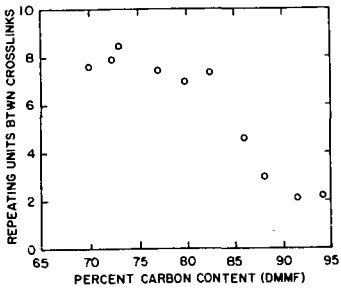

Figure 5. Dependence of Number of Repeating Units Between Crosslinks on Carbon Content of Coal Sample.

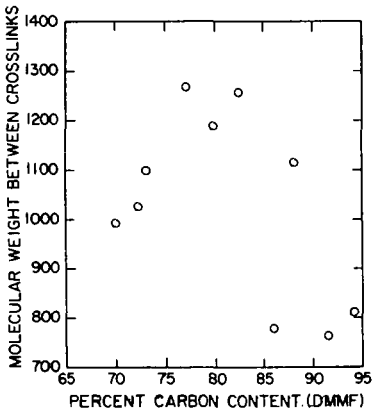

Figure 6. Dependence of Molecular Weight Between Crosslinks on Carbon Content of Coal Sample.

to a value of 2.2 at a carbon content of 91.54%C (dmmf).

Nelson (1983) obtained solvent uptake data for methanol vapor into coal over a range of activities of methanol and then applied modification and rearrangements of the Flory-Rehner network swelling equation and of the modified Gaussian network equation (1) to these results. The modification he made was to assume that the swollen coal system was infinitely dilute in coal, and thus the volume fraction of solvent could be approximated as the activity of the solvent. This is obviously an invalid approximation as the volume fraction of coal in a methanol swelled coal system is on the order of 0.7. He also assumed in his determination of the molecular weight between crosslinks that the number of repeating units between crosslinks was about 7. This defeats the purpose of the modified Gaussian equation, which is to elucidate the effective flexibility or number of repeating units between crosslinks. It is the size of the repeating unit which must be known or estimated. The values of the molecular weight between crosslinks determined by Nelson for swelling by methanol were *ca* 70 and *ca* 120, using the Flory-Rehner and modified Gaussian equations, respectively.

Equilibrium swelling results of pyridine extracted coals in pyridine liquid at room temperature were obtained by Kirov *et al.* (1967). The research group of Sanada and Honda (1966) performed equilibrium swelling of pyridine extracted coals with pyridine vapor at room temperature. Both groups used their data in the Flory-Rehner Gaussian equation. The results have been recalculated (Larsen and Kovac, 1978; Lucht and Peppas, 1981a) to correct some errors in the initial work of Sanada and Honda and to convert the values of volume between crosslinks determined by Kirov *et al.* to the more commonly used molecular weight between crosslinks.

The values of $\overline{M}_c$ determined by us from the data of Kirov *et al.* are 2595, 2100 and 940 for coals with carbon content of 75.9, 82.4 and 88.2%C (daf). The magnitude of the values $\overline{M}_c$ are approximately twice those of our values, which could result from an apparent high degree of swelling due to solvent between particles in the liquid equilibrium swelling procedure used. Our corrected results of the data of Sanada and Honda range from $\overline{M}_c$ equal to zero (a large negative number) to about 15,000, although many of their values of $\overline{M}_c$ range from 700 to 2000. The unreasonable values of $\overline{M}_c$ result from the values they used of the thermodynamic interaction parameter, χ, obtained from the results of osmotic pressure data for pyridine extractables of Wynne-Jones *et al.* (1952). When the value of χ increases for a given set of conditions, the value of $\overline{M}_c$ will also increase until χ reaches a certain critical value, beyond which the Gaussian and the modified Gaussian equations predict a negative molecular weight between crosslinks. Rephrased, it is impossible to have simultaneously a high degree of swelling and unfavorable interaction between a solvent and the macromolecule being swelled.

REFERENCES

Kirov, N.Y., J.M. O'Shea and G.D. Sergent, *Fuel, 46,* 415 (1967).
Larsen, J.W. and J. Kovac, in "Organic Chemistry of Coal," J.W. Larsen, ed., p. 36, ACS Symposium Series No. 71, American Chemical Society, Washington, D.C., 1978.
Lucht, L.M. and N.A. Peppas, in "New Approaches in Coal Chemistry," B. Blaustein, B.C. Bocrath and S. Friedman, eds., ACS Symposium Series, American Chemical Society, Washington, D.C., 43, 1981a.
Lucht, L.M., and N.A. Peppas in "Chemistry and Physics of Coal Uitlization," B.R. Cooper and L. Petrakis, eds., AIP Conference Proceedings, No. 70, p. 28, American Institute of Physics, New York, N.Y., 1981b.
Marzec, A., M. Juzwa, K. Betlej and M. Sobkowiak, *Fuel Process. Tech., 2,* 35 (1979).
Nelson, J.R., *Fuel, 62,* 112 (1983).
Sanada, Y. and H. Honda, *Fuel, 45,* 295 (1966).
Sanada, Y. and H. Honda, *Fuel, 46,* 451 (1967).
Van Krevelen, D.W., "Coal", Elsevier Pubishing Co., New York, N.Y., 1961.
Wiser, W.H., Proceed. Conf. Scient. Probl. Coal Utiliz., DOE Symp. Series, Morgantown, West Virginia, (1977).

Supported by DOE grants Nos. DE-FG22-80PC30222 and DE-F622-78ET13379, and by the Exxon Education Foundation.

REACTIONS OF THE COAL CLEAVING REAGENT, PYRIDINE HYDRIODIDE, WITH ETHERS AND ESTERS

David H. Buchanan, A. Mei-Ying Chen and James N. O. Sy

Department of Chemistry, Eastern Illinois University, Charleston, IL 61920, U.S.A.

INTRODUCTION

Mayo reported(1,2,3) efforts to break cross-links in coal under mild conditions, by treating a toluene insoluble, pyridine soluble (TIPS) fraction of Illinois No.6 coal with pyridine hydriodide (Py-HI) in pyridine, at room temperature, for six days. The hydroxyl content of the product increased, the molecular weight (VPO,GPC) decreased and iodine was incorporated. Lithium iodide in pyridine showed a similar effect. Treatment of TIPS with sodium in liquid ammonia quenched by NH_4Cl also increased the hydroxyl content but the decrease in molecular weight was less than with Py-HI. Treatment of the sodium/ammonia products with Py-HI further reduced the molecular weight. The suggestion is that these reagents are cleaving similar, if not identical, functional groups in coal.

Sodium in liquid ammonia cleaves ethers in coal(4,5), most likely diaryl or aryl-benzyl but not alkyl-aryl or dialkyl ethers, by a radical anion mechanism.(6)

This study was undertaken to determine if ether or ester groups of types which may be present in coal are cleaved by Py-HI or LiI in pyridine, at moderate temperatures, to produce phenols. Py-HBr(7) cleaves alkyl-naphthyl ethers above 230°, but low temperature cleavage reactions with Py-HI have not been reported. Lithium iodide demethylates 2-methoxynaphthalene in refluxing collidine (172°).(8)

Mono-functional ethers or esters treated with Py-HI or LiI in the presence and absence of coal fractions, solvents, sulfides and radical sources are unreactive at low temperatures but alkoxy groups ortho to an aromatic carboxyl group are cleaved.

EXPERIMENTAL

Pyridine hydriodide was prepared in 78% yield by passing HI gas into a dry toluene solution of pyridine and recrystallizing the solid product from methanol. The following compounds were synthesized by standard methods and have physical constants in agreement with literature values: Benzyl phenyl ether (I), 2-naphthylmethyl-2-naphthyl ether (II), 1-naphthylmethyl-1-naphthyl ether (III), cyclohexyl phenyl ether (IV), phenyl phenethyl ether (V), and 1-naphthyl benzoate (VI). Other model compounds were reagent grade commercial products, checked for purity by HPLC and NMR, and used without further purification.

Pyridine was distilled from barium oxide under nitrogen before use. Reactions were usually conducted on a .1-10 mmole scale (.02-.3M), under nitrogen. Products were isolated from pyridine solutions by quenching with aqueous acid followed by extraction and quantitative analysis using either gas chromatography (12% FFAP column) or HPLC (C_{18} reverse phase column). The reported yields (or recoveries) are reproducible within ±3% absolute. Fractions of an Illinois No. 5 coal (PSOC-252) from the Penn State Coal Data Bank were isolated by the methods of Mayo. For experiments in which ethers and Py-HI were mixed with coal fractions, an aspirator vacuum was applied and broken with nitrogen several times to speed up the swelling or dissolution of the fraction and diffusion of reagents into the coal network.

REACTIONS WITHOUT SOLVENT

As expected from Royer's work(7), the following compounds were cleaved by excess Py-HI in an evacuated, sealed tube at 210° for 45 hrs: Anisole, (I), (IV), (V) and

methyl benzoate. From the ether reactions, phenol was isolated; from the ester, benzoic acid. Only trace amounts of alkyl iodides were found since they react with HI at 210° to yield the observed hydrocarbons. These results show the ethers to behave normally and also indicate that the reactivity of Py-HI is slightly greater than that of Py-HBr, as expected for cleavage by nucleophilic substitution. At 196° and 25 hours, Py-HI converted 2-methoxy benzoic acid to a complex mixture of products including several ring iodinated species (mass spec).

REACTIONS IN SOLUTION

As expected, 2-naphthylmethyl-2-naphthyl ether (II) is cleaved by refluxing 57% aqueous HI to yield 2-naphthol. However, at temperatures of 50 to 115°, for up to seven days, Py-HI did not cleave the monofunctional aromatic ethers or esters listed in Table 1 in either wet or dry pyridine, acetonitrile or ethanol. The addition of radical initators, AIBN or benzoyl peroxide, did not produce cleavage, nor did FeS, FeS_2 or $FeCl_2$ added to mimic mineral matter in coal. Added diphenyl sulfide also had no effect.

Ethers (I) and (II) were mixed with Py-HI and TIPS or extracted coal, in pyridine, under nitrogen for up to seven days at 55 or 115°. No cleavage products were detected by HPLC (2% detection limit) and ether (II) was recovered from the coal in high yield.

HYDROGEN BONDED ETHERS

Recent data from Larsen(9) and Gethner(10) indicate that ether oxygen in coal may already be protonated and perhaps activated toward iodide attack. Larsen showed that all hydroxyl groups in coal can be derivatized with bis(tri-n-butyltin)oxide and that each introduced tin atom is within hydrogen bonding distance of another heteroatom. Elemental composition requires that this atom be oxygen. Gethner's FTIR study of D_2O exchanged coal shows that all phenolic hydroxyl groups in Illinois No.6 coal are hydrogen bonded, suggesting that the geometry seen in Larsen's tin derivative is also present in coal itself.

We propose that these results can be explained by structure (VII) in which ether oxygen within a coal cross-link is hydrogen bonded to a phenolic hydroxyl group which is also covalently linked to part of the network. Such ethers may be activated toward iodide attack in pyridine solution where simple ethers would not react.

If a structure such as (VII) were present in TIPS, would it activate the ether toward cleavage by iodide? To answer this, we used 2-methoxy phenol, 2-phenylmethoxy phenol and several alkoxy substituted benzoic acids as model ethers for reactions with Py-HI, LiI and KI in pyridine, acetonitrile and DMSO and found that both 2-methoxy and 2-ethoxy benzoic acid are cleaved by sources of iodide ion in pyridine at 85-115° to produce salicylic acid. The two phenols and the 4-methoxy and 2-phenoxy benzoic acids are inert under these conditions. Results are summarized in Table 2.

The substituted benzoic acids were chosen as compounds in which the effect of internal hydrogen bonding on ether cleavage could be conveniently tested and these results do not imply that ethers cleaved in coal are ortho to carboxylic acids. These results do show that Py-HI and LiI can cleave alkyl-aryl ethers in pyridine if the ether oxygen can be protonated by intramolecular hydrogen bonding. Intramolecular hydrogen bonding in 2-methoxy benzoic acid has been demonstrated in the concentration range of our experiments, conditions where benzoic and 2-methyl benzoic acids are largely dimeric.(11)

Based on fluorescence studies, Ware and co-workers(12) concluded that the carboxyl proton of 3-hydroxy-2-naphthoic acid hydrogen bonds to added pyridine, in toluene solution, without complete ionization of the O-H bond. This implies that the acid proton is available for activating an adjacent ether, possibly as in structure (VIII).

If structures such as (VIII) are present in pyridine solution, and provide conditions sufficient for cleavage, then the reactions with KI and LiI are rationalized. The failure of 4-methoxy benzoic acid to react suggests that electronic effects through the ring are not responsible for the reactions of the ortho isomers. Although kinetics have not been determined, the reaction order methyl>ethyl>>>phenyl is consistent with cleavage via nucleophilic substitution on carbon.

The failure of 2-methoxy phenol and 2-phenylmethoxy phenol to react is a problem, since the hydrogen bond in structures such as (VII) must come from hydroxyl rather than carboxyl to be consistent with Larsen's and Gethner's data. Perhaps the geometry for strong internal hydrogen bonding in the model phenols is not appropriate (five versus six membered ring) or the electronic effect of one oxygen inhibits activation of the adjacent oxygen-carbon bond. Studies of other substituted phenols are currently in progress.

SUMMARY

Pyridine hydriodide and lithium iodide, in pyridine, dealkylate 2-methoxy and 2-ethoxy, but not 4-methoxy benzoic acids at 115°. These results plus the reports of Mayo et al (1,2,3) allow, but do not require, the conclusion that iodide reagents cleave ethers in coal. Based upon the behavior of these and other model compounds, we believe that any ethers in coal cleaved by LiI or Py-HI in pyridine must have structures which provide intramolecular hydrogen bonding to the ether oxygen to activate the oxygen-carbon bond toward attack by iodide ion. Gethner's and Larsen's recent results indicate that ethers in coal may meet this requirement.

ACKNOWLEDGEMENTS

Financial support from the Illinois Coal Research Board and the Faculty Research Council of Eastern Illinois University, plus laboratory assistance from Ken Osborne and Alan Wilcox, is gratefully acknowledged.

REFERENCES

1. Mayo, F.R., Buchanan, D.H. and Pavelka, L.A., Fuel Division, Am. Chem. Soc., Preprints, 1980, 25, No. 2, 182

2. Mayo, F.R., Buchanan, D.H., Pavelka, L.A. and Hirschon, A.S., Manuscript submitted to Fuel

3. Mayo, F.R., Hirschon, A.S., Zevely, J.S., Sundback, K., Fuel Division, Am. Chem. Soc., Preprints, 1983, 28, No. 5, 253

4. Lazarov, L. and Angelova, G., Fuel, 1968, 47, 333

5. Alemany, L.B. and Stock, L.M., Fuel, 1981, 60, 1002

6. Burwell, R.L., Chem. Rev., 1954, 54, 615

7. Royer, R., Buisson, J.P. and Demerseman, P., Bull. Soc. Chim. Fr., 1971, 4362

8. Harrison, I.T., Chem Comm., 1969, 616

9. Larsen, J.W., Nadar, P.A., Mohammadi, M. and Montano, P.A., Fuel, 1982, 61, 889

10. Gethner, J.S., Fuel, 1982, 61, 1273

11. Miller, K.J., J. Chem. and Eng. Data, 1976, 21, 308

12. Ware, W.R., Shukla, P.R., Sullivan, P.J. and Bremphis, R.V., J. Chem. Phys., 1971, 55, 4048

Table 1 Starting material recovery from reactions of Py-HI with model ethers or esters

Compound[a]	Solvent	Catalyst	Time	Temp (°C)	% Recovery[b]
I	Py	None, Ext Coal TIPS	5hr-7d	55-80	89-93
I	Py, CH_3CN	AIBN, $(PhCOO)_2$	1-2d	70-95	87-94
II	Py	FeS, FeS_2, Ph_2S Ext Coal, H_2O, $FeCl_2$	3-7d	90-115	94-100
II[c]	Py	None	5d	90	98
II	CH_3CN	None	5d	78	94
III	Py	None	3d	115	100
IV, V	CH_3CN	None	1, 3d	81	93, 94
VI	Py	None	3d	115	96
Anisole	Py, EtOH	None	5-6hr	Reflux	92-93
Methyl Benzoate	CH_3CN	None	10hr	81	93

a Identified in Experimental Section
b No cleavage products detected (<2%)
c LiI-H_2O in place of Py-HI

Table 2 Reaction of substituted benzoic acids or phenols with iodide salts

Substituent	Reagent	Solvent	Temp[a] (°C)	% Acid Product	% Ether Recovered
Benzoic Acids					
2-methoxy	Py-HI	Py	85	10	80
2-methoxy	Py-HI	Py	115	81	14
2-methoxy	LiI-H_2O	Py	85	54	44
2-methoxy	KI	Py	115	58	33
2-methoxy	Py-HI	CH_3CN	75	--[b]	99
2-methoxy	Py-HI	DMSO	75	--	94
2-ethoxy	Py-HI	Py	115	18	84
2-phenoxy	Py-HI	Py	115	--	100
2-phenoxy	LiI-H_2O	Py	90	--	94
4-methoxy	Py-HI	Py	115	--	96
Phenols					
2-methoxy phenol	Py-HI	Py	115	--	100
2-phenylmethoxy phenol	Py-HI	Py	115	--	100

a Reaction time 3 days
b No cleavage products detected (<2%)

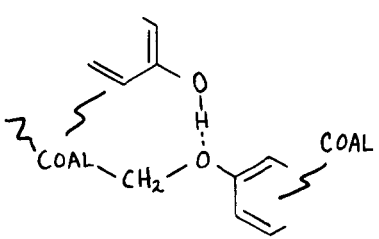

Structure (VII)

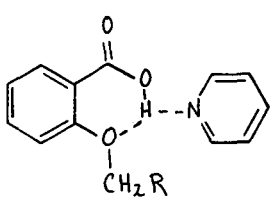

Structure (VIII)

EXPERIMENTAL AND MODELING STUDIES IN FIXED-BED COAL GASIFICATION

B. Joseph, A. Bhattacharya, L. Salam and M. P. Duduković

Chemical Engineering Department
Washington University
Campus Box 1198
St. Louis, MO 63130

ABSTRACT

A laboratory scale fixed-bed coal gasification reactor was built with the objective of obtaining detailed temperature profiles inside the bed during the gasification process. Such data are needed in validating proposed models for fixed-bed gasification and in the estimation of suitable parameters for use with proposed models. This article describes the experimental setup and presents the results of a run using Wyoming coal. The experimental data are compared with simulation results obtained using a detailed two-dimensional model of the gasifier.

1. INTRODUCTION

Fixed-bed coal gasification is a commercially used technology for reacting coal with steam and oxygen to produce useful gases such as CH_4, CO, and H_2. Considerable work has been done lately on modeling of the fixed-bed gasifier. A rather detailed model was presented by Yoon et al. (1). Further improvements on this model have been made by Cho and Joseph (2) and Kim and Joseph (3). It has been difficult to establish the validity of these models fully because of the lack of sufficient operational data on commercial scale gasifiers. The research presented here was undertaken to remedy this situation by developing an experimental procedure for generating data which can be used directly in the verification of proposed models and to determine parameters that are required in the model. The paper contains a detailed description of the apparatus used, the experimental procedure and selected results on gasification of Wyoming coal. The paper also includes a brief sketch of the modeling effort and a comparison between the experimental data and model predictions.

2. DESCRIPTION OF EXPERIMENTAL SETUP

In a commercial scale fixed-bed gasifier, coal is fed continuously at the top at a slow rate while steam and oxygen (or air) is fed at the bottom. The coal undergoes drying and devolatilization at the top of the gasifier and char descends slowly through the reactor. Because the char-bed is moving slowly it is termed as a fixed-bed reactor. For the purposes of this research it was decided that the runs will be conducted on a bed of char which is stationary. Hence it approximates the commercial process with the coal feed cut off. The resulting transient data (since we will have a reaction front moving through the char bed) is then used for validating models of gasifiers.

Figure 1 shows the schematic of the experimental setup. The major pieces of equipment are a steam generator, feed preheater, the tubular reactor, a condenser for removing tars and water, gas chromatograph for product gas analysis and a data acquisition system for monitoring the temperature.

The gasification vessel is a 4 in. diameter, 4 ft. long cylindrical stainless steel tube insulated with refractory and surrounded by a 6 inch diameter stainless steel tube. The vessel can be operated at temperatures as high as 1200°C. This reactor is packed with devolatilized coal. The

devolatilization is carried out separately in another furnace in a nitrogen atmosphere at a temperature of approximately 800°C until no further weight loss occurs. The coal used is in the size range 8 - 20 mesh (2.3 - .833 mm). Each run requires approximately 4 kg of coal. A superficial gas velocity of approximately 1 ft/sec is used in the gasifier.

Figure 2 shows a detail of the gasification reactor. The reactor is designed to operate close to atmospheric pressure. Heat losses are minimized by a refractory lining around the reactor tube and by ceramic beads at both ends of the tube. An ignition coil at the top of the bed is used to start the combustion reaction. Initially the inside liner of the gasifier was constructed with ceramic but it cracked repeatedly due to thermal shock.

The product gases are sent through a condenser and liquid separator to remove water, tar and ash. The remaining gases are flared. A sample is sent through the GC for analysis every 15 minutes.

Temperature profiles in the bed are measured by means of two thermowells inserted axially at r = 0 and r =.36 cm. Type K (chromel/alumel) thermocouples were used. The thermocouple locations are shown in Figure 2. The data from the thermocouples was collected by means of an LSI/11 microcomputer and stored on tape. This data was then transmitted to a DEC-20 mainframe where the data is analyzed further.

3. EXPERIMENTAL RESULTS

Two successful runs were made using char generated from Wyoming coal. The results of the second run are reported here. The coal analysis is given in Table 1. The operating conditions of the gasifier are reported in Table 2. Note that the air flow had to be decreased after 45 minutes to maintain the maximum temperatures below 1200°C. The run was terminated after 50 minutes. An analysis of the material remaining in the gasifier indicated some unconverted carbon (see Table 2). The bed length was only 12 cm indicating that the ash collapsed.

The results of the run are shown in Figures 3, 4 and 5. Figure 3 shows the temperature profiles of the inner thermocouples. Note that after the temperature has reached a peak, the thermocouple is sitting in a bed of ash and the drop in termperature is caused by heat loss from the bed to the walls and the gases. The peak temperatures are around 1200°C and the peak value decreases as the bed is reacted. Also there is a considerable spreading of the profile in the axial direction towards the end of the run.

Figure 4 shows the temperature profiles of the outer thermocouples. These temperatures are notably lower than the inner ones. This is not surprising since the wall acts as a heat sink lowering the temperatures close to the wall. Also the spreading of the temperatures in the axial direction is seen in this set of profiles also.

Figure 5 shows the product gas composition as a function of time. After the initial transient the composition attains nearly constant values. There is some oxygen bypassing in the gasifier. The fluctuations are probably caused by errors in analysis. Due to the use of helium as the carrier gas in the gas chromatograph, hydrogen analysis had a large correction factor and hence has greater error than the other gases. Attempts on closing a hydrogen mass balance around the system confirmed this.

Whether or not the oxygen bypassing occured through the bed or the insulated wall is difficult to determine. As the reaction progresses, the bed length decreases and hence the associated pressure drop through the bed also decreases. This might have contributed to decreased bypassing of the oxygen.

4. COMPARISON WITH SIMULATION RESULTS

In parallel with this experimental investigation, a modeling study was conducted with two objectives. The first was to be able to study the behavior of large scale fixed-bed gasifiers such as the Lurgi-type. The second was to be able to validate the model using the results from the laboratory scale gasifier. The details of the model was published elsewhere (Joseph, et al., 1983). A brief summary is given here.

In a typical commercial scale gasifier the coal is moving at a much smaller velocity than the gases. As a result, the gasifier can be divided into two zones, one for drying and devolatilization and another for combustion and gasification. The first zone is relatively narrow and can be assumed to take place instantaneously for practical purposes. It is the second zone that determines the operating characteristics of the gasifier. In this zone, char descends slowly reaching with the gases rising from the combustion zone. This was the reason for using char instead of coal in the experimental studies. The main reactions in this zone are char-oxygen, char-steam, char-carbon dioxide and the water-gas shift reaction. In addition to these reaction kinetics, the heat and mass transfer in both axial and radial directions play a significant role.

A number of assumptions are required to develop a model that is both mathematically and computationally tractable. Some major assumptions include a shrinking-core model for gas-solid kinetics, no axial dispersion of heat and a homogeneous gas-solid temperature in the bed. The equations resulting from the mass and energy balances are solved numerically using suitable integration methods. The interested reader is referred to Joseph et al. (4).

Figures 6 and 7 show a comparison of temperatures predicted by the model and those experimentally observed. The agreement between the two during the early part of the run is good. However the temperature profiles predicted by the model tend to be rather uniform with respect to time whereas the experimental profiles exhibit a marked decrease in the peak value and a spreading of the profile in the axial direction.

Similar trends were observed in another run as reported in Salam (5). This spreading of the temperature profile could have been caused by a number of reasons. Sources of modeling errors include (i) axial dispersion of heat (ii) thermal storage and conductivity of the thermowells (iii) reduction in bed length caused by collapsing ash layer (iv) effect of heat transfer by radiation to the walls and (v) effect of channeling and bypassing of oxygen through the bed.

5. CONCLUSIONS

This paper presented the results of a char gasification run using Wyoming coal in a fixed-bed laboratory gasifier. The temperature profiles in the bed at various axial and radial positions are presented as a function of time. The results are useful in validating proposed models for fixed-bed gasifiers. Comparison with one such model indicates that the model is capable of predicting

the initial temperature profiles reasonably well, but requires further refinement to be able to explain some flattening trends in the temperatures. Current research is focused on trying to update the model in order to explain the experimental observations.

6. REFERENCES

1. Yoon, H., J. Wei and M. M. Denn, "Model for Moving-Bed Coal Gasification Reactors", AIChE Journal 24, p. 885 (1978).

2. Cho, Y. S. and B. Joseph, "A Heterogeneous Model for Moving-Bed Coal Gasifiers", Industrial and Engineering Chemistry, Process Design and Development, Vol. 20, 318 (1981).

3. Kim, M. and B. Joseph, "Dynamic Modeling of Moving-Bed Coal Gasifiers", Industrial and Engineering Chemistry, Process Design and Development, Vol. 22, 212 (1983).

4. Joseph, B. A. Bhattacharya, L. Salam and M. P. Duduković, "Modeling and Simulation of Fixed-bed Coal Gasification Reactors, Systems Simulation of Fossil Energy Processes", Symposium organized by Morgantown Energy Technology Center, Department of Energy, Morgantown, West Virginia (Dec., 1983). Proceedings to appear.

5. Salam, L., "An Experimental Investigation of Fixed-Bed Coal Gasification", M.S. Thesis, Washington University, St. Louis (August, 1983).

Coal Analysis

Mine	Wyodak
Town	Campbell
County	Campbell
State	Wyoming
Abbreviated ID	Wyo 1
Sample Date	7-15-78
Bin #	3500

Proximate Analysis:
As Received

Moisture	31.87
Volatile Matter	32.46
Fixed Carbon	30.16
Ash	5.51
Heating Value (Btu/lb)	7978

Ultimate Analysis:
Moisture-free

Ash	8.09

Moisture- and Ash-free

Hydrogen	5.75
Carbon	74.05
Nitrogen	1.39
Sulfur	0.53
Oxygen (by diff)	18.28
Heating Value MAF (Btu/lb)	12,742
H/C Ratio	0.93

Table 1. Analysis of Coal Used in the Gasification Runs

Char Loaded:	3645.7 gms devolatilized Wyodac char		
Char Composition:	83.56% Carbon		
	11.97% Ash		
	2.33% Oxygen	> Moisture included	
	1.02% Hydrogen		
	0.62% Nitrogen		
	0.50% Sulfur		
Time 0-45 min.			
INLET	Air Flowrate:	1.478	m^3/hr*
	Water Flowrate:	3.48	gm/min
	O_2/H_2O:	2.12	gm/gm (1.192 mol/mol)
OUTLET	Product Gas Flowrate:	2.055	m^3/hr*
	Total Condensate:	0	gm
Time 45-580			
INLET	Air Flowrate:	1.206	m^3/hr*
	Water Flowrate:	3.48	gm/min
	O_2/H_2O:	1.73	gm/gm (0.975 mol/mol)
OUTLET	Product Gas Flowrate:	2.022	m^3/hr*
	Total Condensate:	382.2	gms
Unreacted Carbon:	697.8 gms		
Reactor Pressure:	0.1910 MPa		
Original Bed Length:	85.7 cm		
Final Bed Length:	approximately 12.0 cm		

* at 25°C, 0.1013 MPa

Table 2. Summary of Operating Conditions for Gasification Run #072483

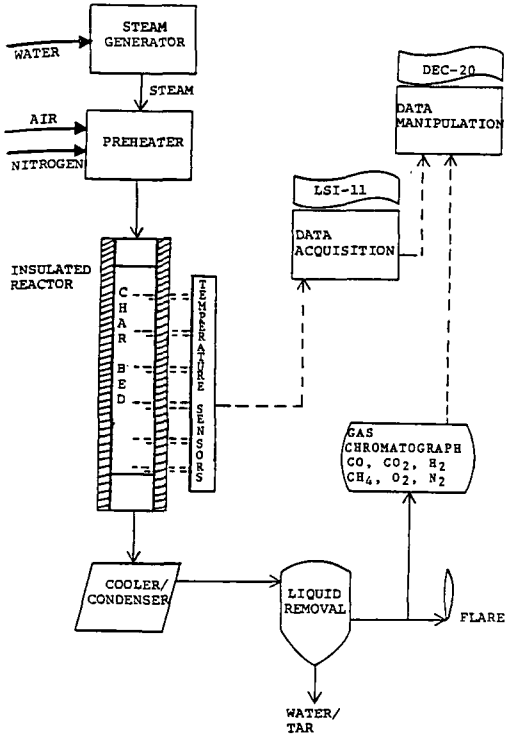

Figure 1. Schematic of Experimental Setup

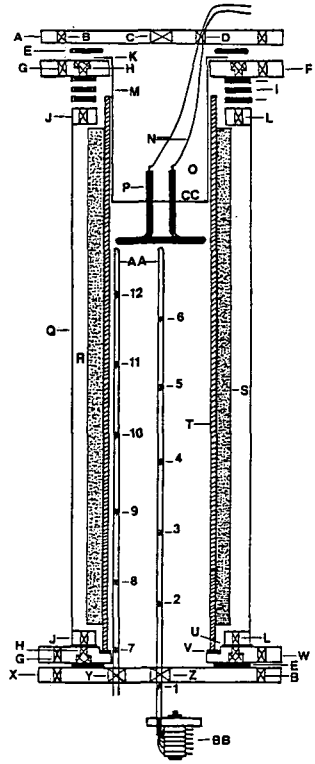

Figure 2. Detail of Gasification Vessel.
See next page for Legend.

A	- 1 cm thick x 19 cm diameter 304 stainless steel top cover
B	- 6 - bolt holes
C	- 1/4" FPT for stainless steel inlet fitting (centered)
D	- 1/4" FPT for stainless steel ignition lead fitting (2 cm from center)
E	- 1/8" (0.3175 cm) compressed asbestos (casp) gasket seals basket flange bolt holes H and cover
F	- 19 O.D. x 7.75 cm I.D. steel top flange 1 cm thick
G	- 6 - 1/4"-20 threaded bolt holes
H	- 6 - recessed bolt holes
I	- 3 - 1/8" casp gasket seals and shims top flange
J	- 14.9 O.D. x 11.6 cm I.D. steel retaining flanges (1 cm thick) welded inside each end of steel shell
K	- 10.8 O.D. x 7.6 cm I.D. stainless steel basket flange (0.0051 cm thick) welded to basket
L	- 6 - 1/4"-20 threaded bolt holes
M	- 12.7 x 10 cm stainless steel sheet (0.0051 cm thick) rolled and welded to form a 7.6 cm diameter tube for basket wall
N	- Asbestos braided copper ignition leads
O	- 1/2" (1.27 cm) Diamonite (95% alumina grinding media) ceramic beads
P	- 1/4" x 12" (0.635 x 30.4 cm) Incoloy sheathed tubular heater bent to form 5.7 cm loop with 7 cm perpendicular legs
Q	- 6" O.D. x 47.7" (15.24 x 121.2 cm) steel pipe for outside wall (0.1651 cm wall)
R	- 1" x 24" x 48" (2.54 x 60.96 x 121.92 cm) Kaowool 2600 refractory blanket wraps liner twice
S	- Preformed refractory sleeves (Kaowool 2600), split and slid over liner. Refractory cement fills resulting gap
T	- 3-3/4" O.D. x 48" (9.525 x 121.92 cm) 304 stainless steel liner (0.3048 cm wall)
U	- 1/8" casp gasket seals bottom flange
V	- 1/8" casp gasket seals liner bottom
W	- Bottom flange same as F with 9.75 cm shoulder 7 mm deep
X	- Same as A for bottom cover
Y	- 1/8" FPT for stainless steel thermowell fitting
Z	- 1/4" FPT for stainless steel exit and thermowell tee fitting
AA	- 3/16" O.D. (0.4762 cm) Inconel thermowells 117 and 122 cm
BB	- Aluminum thermocouple plug mounting block with set screw
CC	- Perforated stainless steel basket bottom (4 x 7/32" holes/inch)

Thermocouple Locations From Top of Well (Bed)

1.	113.0 cm	7.	105.1 cm
2.	91.8 cm	8.	85.7 cm
3.	71.1 cm	9.	65.7 cm
4.	51.1 cm	10.	44.4 cm
5.	29.8 cm	11.	24.3 cm
6.	11.0 cm	12.	4.8 cm

Note all thermocouples are 0.02" (0.0508 cm) diameter Inconel sheathed chromel/alumel rated at 1150°C.

Legend for Figure 2

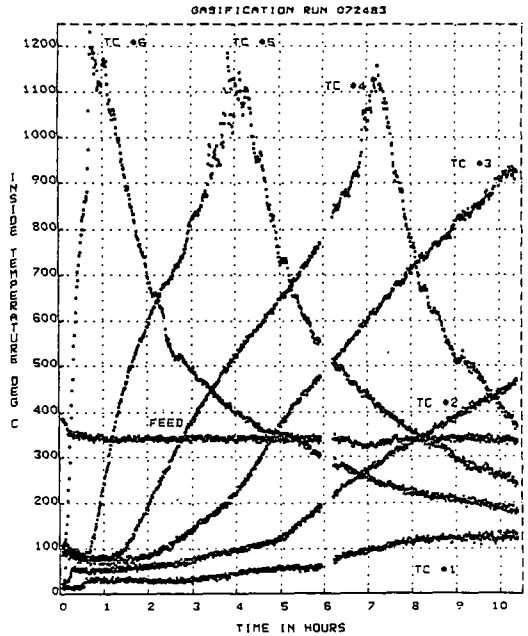

Figure 3. Temperature Profiles in the Gasifier (Central Thermowell)

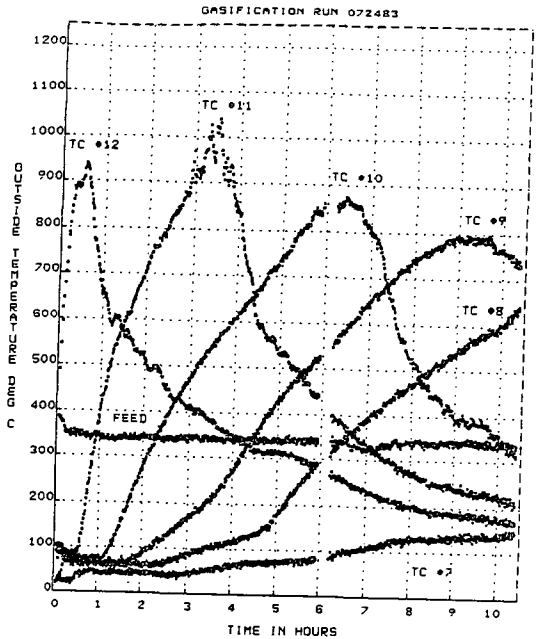

Figure 4. Temperature Profiles in the Gasifier (Thermowell near the Wall)

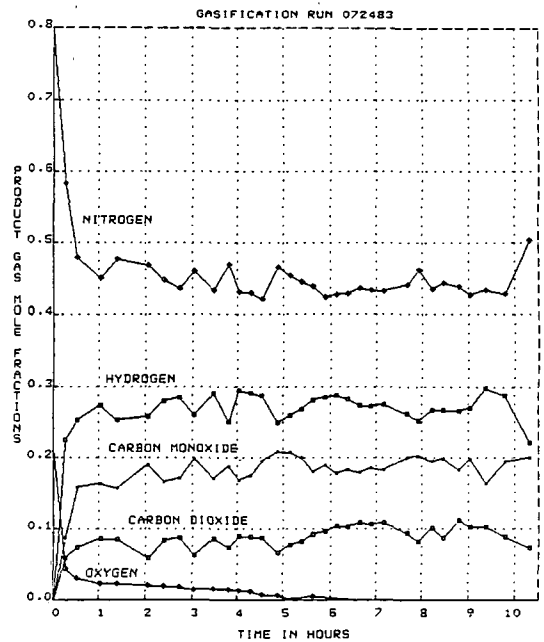

Figure 5. Product Gas Composition as a Function of Time

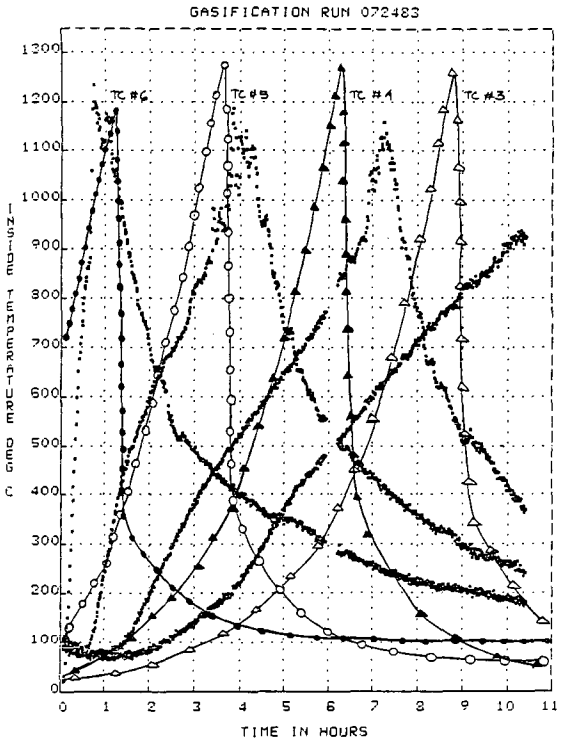

Figure 6. Comparison of Temperature Histories at Thermocouple Locations, Inner Thermowell. Straight Lines are Model Predictions.

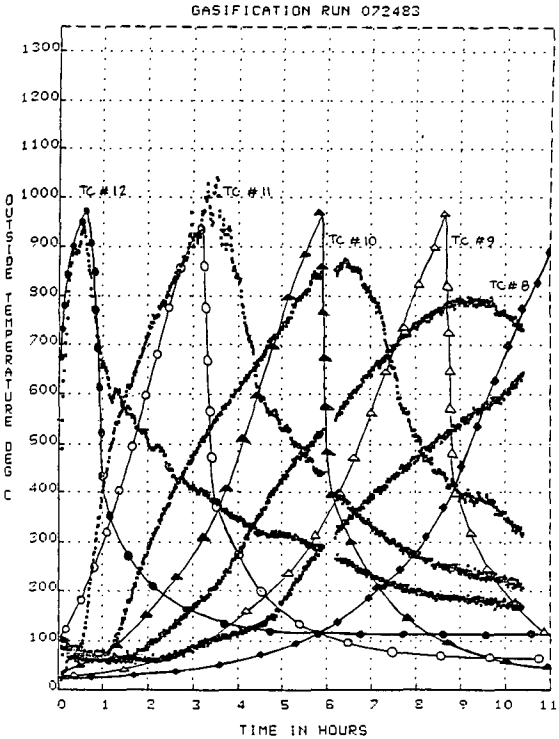

Figure 7. Comparison of Temperature Profiles for the Thermocouples near the Wall. Straight Lines are Model Predictions.